**SANDIA REPORT**
SAND2013-4494
Unlimited Release
Printed May 2013

# Composite $WO_3/TiO_2$ nanostructures for high electrochromic activity

Karla R. Reyes, Zachary D. Stephens, and David B. Robinson

Prepared by
Sandia National Laboratories
Albuquerque, New Mexico 87185 and Livermore, California 94550

Sandia National Laboratories is a multi-program laboratory managed and operated by Sandia Corporation, a wholly owned subsidiary of Lockheed Martin Corporation, for the U.S. Department of Energy's National Nuclear Security Administration under contract DE-AC04-94AL85000.



Issued by Sandia National Laboratories, operated for the United States Department of Energy by Sandia Corporation.



Available to DOE and DOE contractors from
U.S. Department of Energy
Office of Scientific and Technical Information
P.O. Box 62
Oak Ridge, TN 37831
Telephone: (865) 576-8401
Facsimile: (865) 576-5728
E-Mail: reports@adonis.osti.gov
Online ordering: http://www.osti.gov/bridge

Available to the public from
U.S. Department of Commerce
National Technical Information Service
5285 Port Royal Rd.
Springfield, VA 22161
Telephone: (800) 553-6847
Facsimile: (703) 605-6900
E-Mail: orders@ntis.fedworld.gov
Online order: http://www.ntis.gov/help/ordermethods.asp?loc=7-4-0#online

SAND2013-4494
Unlimited Release
Printed May 2013

# Composite $WO_3/TiO_2$ nanostructures for high electrochromic activity

Karla R. Reyes*, Zachary D. Stephens*, and David B. Robinson†
Materials Chemistry (8223)* and Energy Nanomaterials (8651)†
Sandia National Laboratories
P.O. Box 969
Livermore, California 94551-MS9403

## Abstract

A composite material consisting of $TiO_2$ nanotubes (NTs) with $WO_3$ electrodeposited homogeneously on its surface has been fabricated, detached from its substrate, and attached to a fluorine-doped tin oxide film on glass for application to electrochromic (EC) reactions. A paste of $TiO_2$ made from commercially available $TiO_2$ nanoparticles creates an interface for the $TiO_2$ NT film to attach to the FTO glass, which is conductive and does not cause solution-phase ions in an electrolyte to bind irreversibly with the material. The effect of NT length on the current density and the EC contrast of the material were studied. The EC redox reaction seen in this material is diffusion- limited, having relatively fast reaction rates at the electrode surface. The composite $WO_3/TiO_2$ nanostructures showed higher ion storage capacity, better stability, enhanced EC contrast and longer memory time compared with the pure $WO_3$ and $TiO_2$.

# Contents

# Figures

# Tables

# 1. Introduction

Electrochromic (EC) materials respond to an applied bias by reversibly changing their spectral absorption properties via a redox reaction. EC materials are of particular interest for their use in smart windows and displays [1]. Smart windows equipped with EC materials give the user the ability to optimize the building's energy use by controlling the amount of light and heat that passes through the window. The largest factor in a building's energy loss to its environment is through its windows; consequently, EC smart windows can decrease the energy used to heat and cool a building by 25%, they can reduce lighting energy requirements by 50%, and they can reduce peak power by 30–40% [1]. EC technology also finds uses in indoor applications, such as UV protection for museum display cases and for privacy purposes in offices and bathrooms. Commercial smart windows (or dynamic windows) still cost up to $1,000 per $m^2$ of glass. The dynamic layers of the EC windows are manufactured with a vacuum depositing process called sputtering. This technique provides a high degree of control and creates uniform results; however, sputtering is expensive, relatively slow, and energy-intensive. Cheaper materials and manufacturing process are needed to make the electrochromic devices a more attractive commercial option.

Wide-bandgap metal oxides, such as $WO_3$, $Nb_2O_5$ and $TiO_2$, are good candidates for EC devices because their well-defined lattice structures allow easy field-aided ion intercalation, which is needed to accommodate the change in oxidation state in the EC material. In addition, they can be manufactured using low-cost processes such as electrodeposition. Of the transition metal oxides, $WO_3$ shows the best EC activity, i.e., it has the highest optical contrast, the lowest onset potential, and has sufficient cycling durability [2] [3] [4]. $WO_3$ is pale yellow, and turns dark blue when partially reduced to $WO_2$. Yu et al. reports a method of electrodepositing thin films of $WO_3$ onto ITO glass and Ni sheets with good optical contrast, smooth morphology, and good durability after 10,000 cycles [5]. De Tacconi et al. used pulsed cathodic electrodeposition to create composite $WO_3/TiO_2$ films on conductive glass with small amounts of $TiO_2$ (W:Ti= 98:2 atom % and W:Ti= 96:4 atom %). They found that composite $WO_3/TiO_2$ has superior coloration/de-coloration dynamics and the blue shift is more pronounced than that of pure $WO_3$ or $TiO_2$ [6].

Nanostructures have been investigated in order to enhance the EC contrast. The ion intercalation is limited to a very thin surface layer of the electrochromic material. Therefore, materials with high surface area could enhance the EC contrast. Porous $WO_3$ can be fabricated that has superior EC properties over compact $WO_3$ [7]. Another interesting morphology with high surface area is one-dimensional nanostructures, such as nanotubes and nanorods. However nano-tubular $WO_3$ cannot be fabricated easily [7], [8], and therefore the morphological advantages of NTs are not retained with $WO_3$. A strategy explored by Benoit et al. dip coats $TiO_2$ NTs with a solution of $WCl_6$ to get, after annealing, an inhomogeneous coat of monoclinic $WO_3$ on the surface of the NT array. EC activity was measured *in situ* while the film was on the Ti substrate, and the $TiO_2$

NTs with $WO_3$ on the surface had increased current densities, more distinct onset potentials, higher contrast, and higher ion intercalation capacity compared to pure $TiO_2$ NTs [8]. The $TiO_2$ NT-$WO_3$ current density of the anodic peak increased by about 1 mA $cm^{-2}$ compared to pure $TiO_2$ NTs, reaching values up to 1.25 mA/$cm^2$ at a scan rate of 50 mV/s in 0.1 M $HClO_4$ electrolyte. The reflectance at 600 nm showed a 3 % on-vs.-off difference for pure $TiO_2$ NTs, a 21 % difference for annealed $TiO_2$ NT-$WO_3$, and a 45 % difference for amorphous $TiO_2$ NT-$WO_3$ [8]. Lai et al. sputter deposited W onto a $TiO_2$ NT array without breaking the well-oriented, vertically aligned nanotubes; this material has a photocurrent density of 1.55 mA $cm^{-2}$, but it was not tested for electrochromic applications.[9]. Nah et al. showed that composite $TiO_2$-$WO_3$ NTs can be fabricated by anodization of a TiW alloy. Their material, tested *in situ* on the TiW alloy substrate, has an ion storage capacity of 16.9 mC $cm^{-2}$ for the anodic process and a reflectance difference of 0.61 [10].

This work shows a low-cost synthetic approach to prepare electrochromic films with organized nanostructures than enhances the ion capacity, EC contrast and stability. This report presents the fabrication, detachment, and transfer to fluorine-doped tin oxide (FTO) glass of a material with high EC activity made of a layer of $TiO_2$ NTs with $WO_3$ electrodeposited on the surface. These materials maintain the morphological advantages of $TiO_2$ NTs while exploiting the superior EC activity of $WO_3$. $WO_3/TiO_2$ materials show anodic peak current values up to 10 mA/$cm^2$ at 40 mV/s scan rate, electrochromic contrast of almost 100% and excellent cycle stability, demonstrating a significant improvement compared to prior materials. The films are successfully transferred to FTO glass for all the EC characterization techniques. This approach has a big commercial potential for EC smart-glass industry because it produces efficient materials with low manufacturing cost. In addition, the EC films can be incorporated to different substrates including existing windows, which could reduce installation costs.

# 2. Materials and procedures

## 2.1 Preparation of composite $WO_3/TiO_2$ nanostructures

### *2.1.1 Preparation, detachment, and transfer of $TiO_2$ NTs*

Ti foil (0.25 mm and 99.7% trace metal basis, Aldrich) was cleaned with acetone, deionized water, and methanol and then dried under a stream of $N_2$ gas. Ti foil was cut in pieces of 2 by 4 cm, and the back of the foil was covered with insulating tape. The Ti foil was used as the anode and Pt gauze as the cathode. A Teflon beaker was used as electrochemical cell and the electrolyte solution used was $NH_4F$ (0.3 wt. %) in ethylene glycol (EG)/water (ratio of 95:5). The reaction was driven by a dc power supply. All the experiments were carried out at room temperature. The $TiO_2$ NTs used for the following reactions were prepared via a two-step process. In the first step (pretreatment), a Ti foil was anodized at 50 V overnight (approximately 15 hours). Then the nanotube layer was removed ultrasonically in deionized water and the remaining foil was dried under a stream of $N_2$ gas. In the second step, the pretreated foil was anodized again with fresh $EG/NH_4F/H_2O$ solution at 50 V. The anodization time was changed to grow NTs of varying lengths to investigate the effect of these different lengths on the material's EC properties. The $TiO_2$ nanotubes were annealed in air at 500 °C for 2 hours to convert the material from an amorphous phase to crystalline anatase.

The membrane was detached from the foil by anodizing for 0.5 hour in the same solution at 50 V to create an amorphous layer of $TiO_2$, and then the sample was exposed to 0.05 wt. % HF to selectively dissolve the amorphous layer, leaving a crystalline $TiO_2$ NT film. The membrane was submerged in NaOH (0.1 M) to neutralize the pH and it was cleaned with DI water. The $TiO_2$ NT membrane was subsequently attached to a conductive fluorine-doped tin oxide film (FTO) on glass using one of a variety of techniques. The following solutions or pastes were investigated to find a conductive and transparent interface to attach $TiO_2$ NT films onto FTO glass:

1. $TiO_2$ P25 paste: 5 g $TiO_2$ nanopowder (Degussa P25) were mixed with 0.5 mL acetic acid and 8 mL DI water, in a ceramic mortar using a pestle. The acetic acid causes strong bonds with the conductive glass [11]. The paste was then ground with a pestle in a mortar for 15 minutes. During this procedure, it is important to ensure the mixing and grinding times are enough to avoid producing a non-homogeneous paste [11].
2. 0.1 M Ti-isoproproxide in 2-propanol.
3. $Ti(OBu)_4$.
4. $TiO_2$ P25 paste with different amounts of $Ti(OBu)_4$ and polyethylene glycol 300 (PEG).

A layer of paste or liquid was coated onto the FTO glass by tape casting and the membrane was transferred onto the glass using the paste as an interface. The $TiO_2$ NT-FTO glass samples were

successively annealed at 423 K for 30 min then 723 K for 1 hour to evaporate any solvents and create an anatase $TiO_2$ layer within the membrane/glass interface [12].

### 2.1.2 $WO_3$ electrodeposition

$WO_3$ was electrodeposited *in situ* while the $TiO_2$ NT membrane was attached to the FTO glass. The deposition solution was prepared by dissolving $Na_2WO_4$ salt (Aldrich) in deionized water and adding concentrated hydrogen peroxide (30%) which can bind to the anion and improve its solubility at low pH. The salt concentration was 25 mM and hydrogen peroxide concentration was 30 mM. The pH of the resulting solution was 10.4 ± 0.1. Nitric acid was added subsequently in order to adjust the pH to 1.4. The solution was prepared the day of the deposition experiments. Either insulating tape or Hysol IC epoxy was used to cover everything except the $TiO_2$ NTs area that was to be electroplated with $WO_3$. A digital photograph was used to calculate the area using ImageJ software. The electrodeposition experiments were performed in a three-electrode Teflon electrochemical cell at room temperature. The reference electrode was Ag/AgCl and the counter electrode was a Pt gauze. A potentiostat (SP-200, Bio-Logic Science Instruments) was used to apply a potential of -0.437 V vs. Ag/AgCl (-0.24 V vs. NHE) and record the charge density during the deposition experiments. The resulting composite materials were annealed in air at 400 °C for 2 hours to yield crystalline $WO_3$. For comparison purposes, the same $WO_3$ electrodeposition procedure and annealing process were followed using $TiO_2$ NTs on either Ti foil or FTO glass as the substrates.

## 2.2 Characterization

The samples on the foil and on the FTO glass were analyzed by scanning electron microscopy-energy-dispersive X-ray spectroscopy (SEM-EDS) and X-ray diffraction (XRD). Morphological characterization was carried out by JEOL JSM7600F Thermal Field Emission SEM. Top views of the $TiO_2$ NTs were taken before and after $WO_3$ electroplating. For the cross-sectional views, the foil was bent and the glass was broken by tracing a scratch with diamond pen and then applying pressure. Several areas of the film were analyzed using an EDS (Oxford XMax with 80mm² detector) that was coupled to the SEM. Crystal structures were collected by Empyrean X-ray diffraction spectrometer and data was analyzed by X'Pert High Score Plus software.

## 2.3 Testing of Electrochromic Properties

For electrochromic measurements, the samples were placed into an electrochemical cell filled with 0.1 M $HClO_4$. Opposite the sample (approximately 3 cm away), a Pt gauze and Ag/AgCl electrode were used as counter and reference electrode, respectively. A SP-200 potentiostat (Bio-Logic Science Instruments) was used to control the parameters and collected the data. Ion storage capacity was determined by cyclic voltammetry. Switching speed was qualitatively analyzed by double potential step chronoamperometry (DPSC).

For the optical properties, the absorption spectra of the films were collected using a Shimadzu UV-2101PC spectrometer with a diffuse reflectance adapter. An initial spectrum was taken for each sample. Then, after the electrochromic switching, the samples were placed in the spectrometer and data was collected at 5-minute intervals. The electrochromic contrast was calculated, subtracting the initial and colored spectra. Memory time was calculated taking the time elapsed from the colored state to back to the initial state at open circuit.

# 3. Results and discussion

## 3.1 Preparation of composite $WO_3$/ $TiO_2$ NTs

Figure 1 shows the synthetic approach taken to develop the composite materials. Parallel approaches were developed to prepare $WO_3/TiO_2$ NTs on Ti foil and on FTO glass (or other substrates). The following section discusses the details of each step of the synthetic approach.

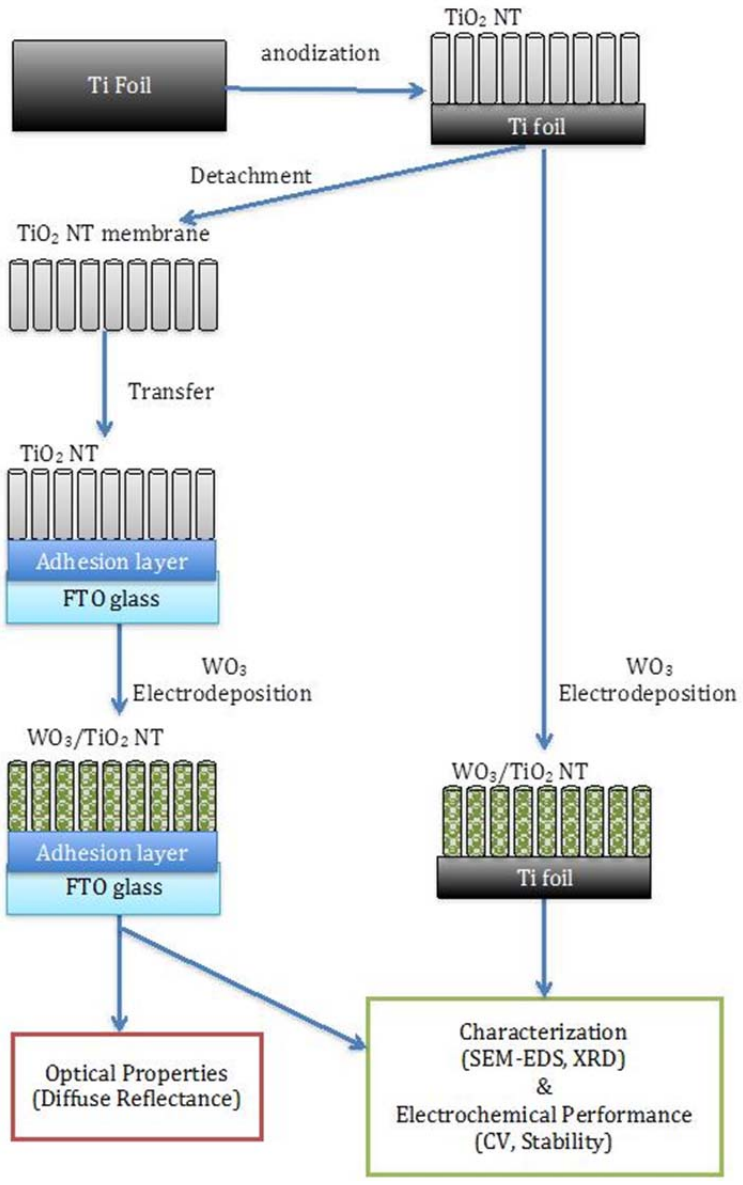


**Figure 1.** Scheme of research approach to prepare composite $WO_3/TiO_2$ NTs.

### 3.1.1 $TiO_2$ NTs preparation

SEM images showed that after the first anodization, the $TiO_2$ nanotubes are in a disordered array due to the corrugated surface of the Ti foil. Figure 2(a-b) shows that, below the disordered surface, the $TiO_2$ NTs are very organized. Several pretreatment techniques have been reported, including acid treatment and polishing; however, a better technique for this approach was to peel off the first $TiO_2$ NT layer and repeat the anodization process [2]. After the nanotube layer was removed ultrasonically, an imprint pattern was left on the foil (Figure 2(c)), which works as template in the further growth of well-aligned nanotubes. After the second anodization, $TiO_2$ NTs are highly uniform and vertically oriented; the opening (mouth) is 100 nm in diameter and the walls are approximately 10 nm thick, as shown in Figure 2(d).

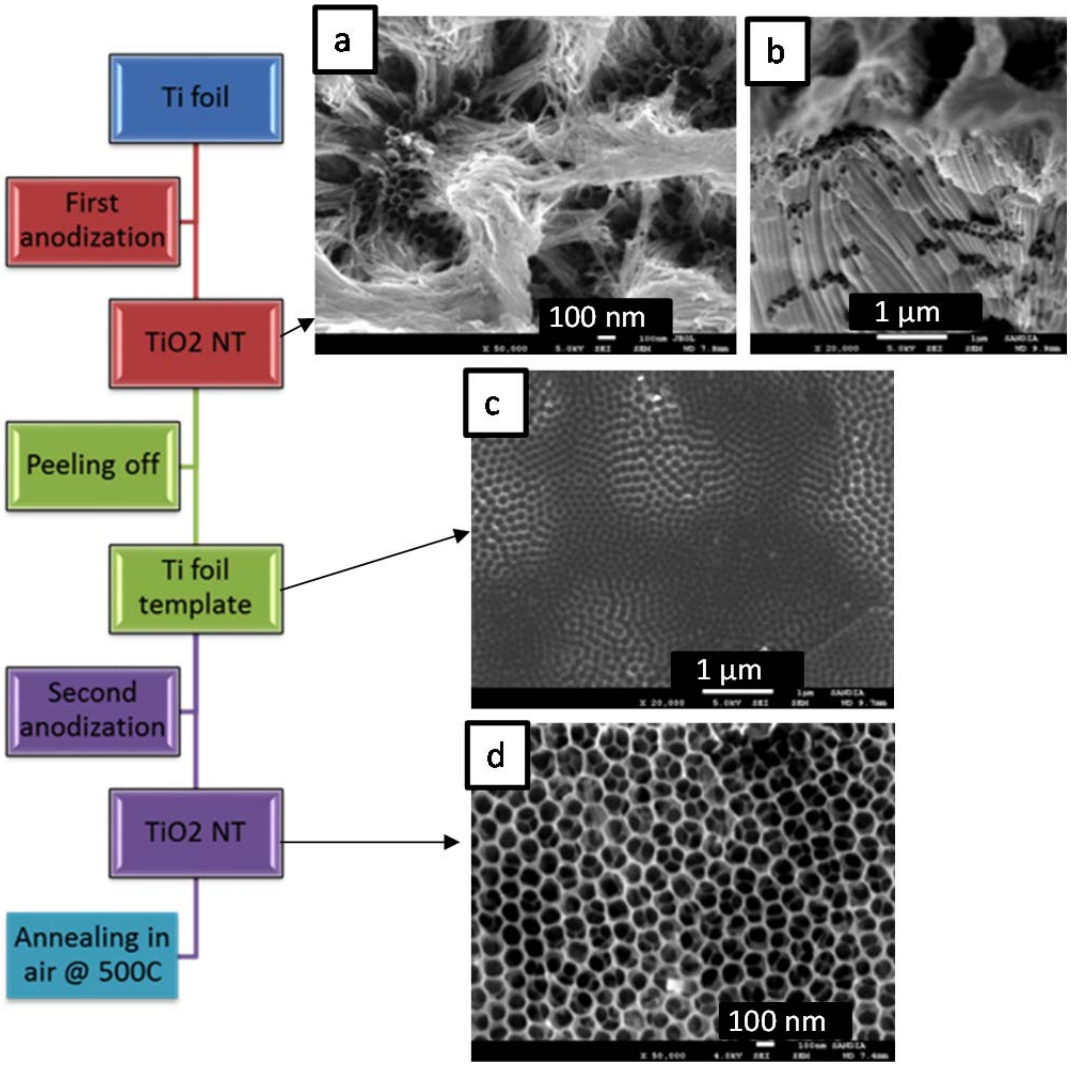


**Figure 2.** Scheme of $TiO_2$ NTs preparation and SEM images at each step: (a) top view and (b) 45° angled view after the first anodization. (c) Imprint pattern after the first $TiO_2$ NTs were removed. (d) Top view after the second anodization.

Figure 3 shows the XRD patterns after the first and the second anodization. Both patterns showed a $TiO_2$ anatase phase, even though the peak intensity and ratio changed from one to the other. Some peaks from the Ti foil (substrate) were detected.

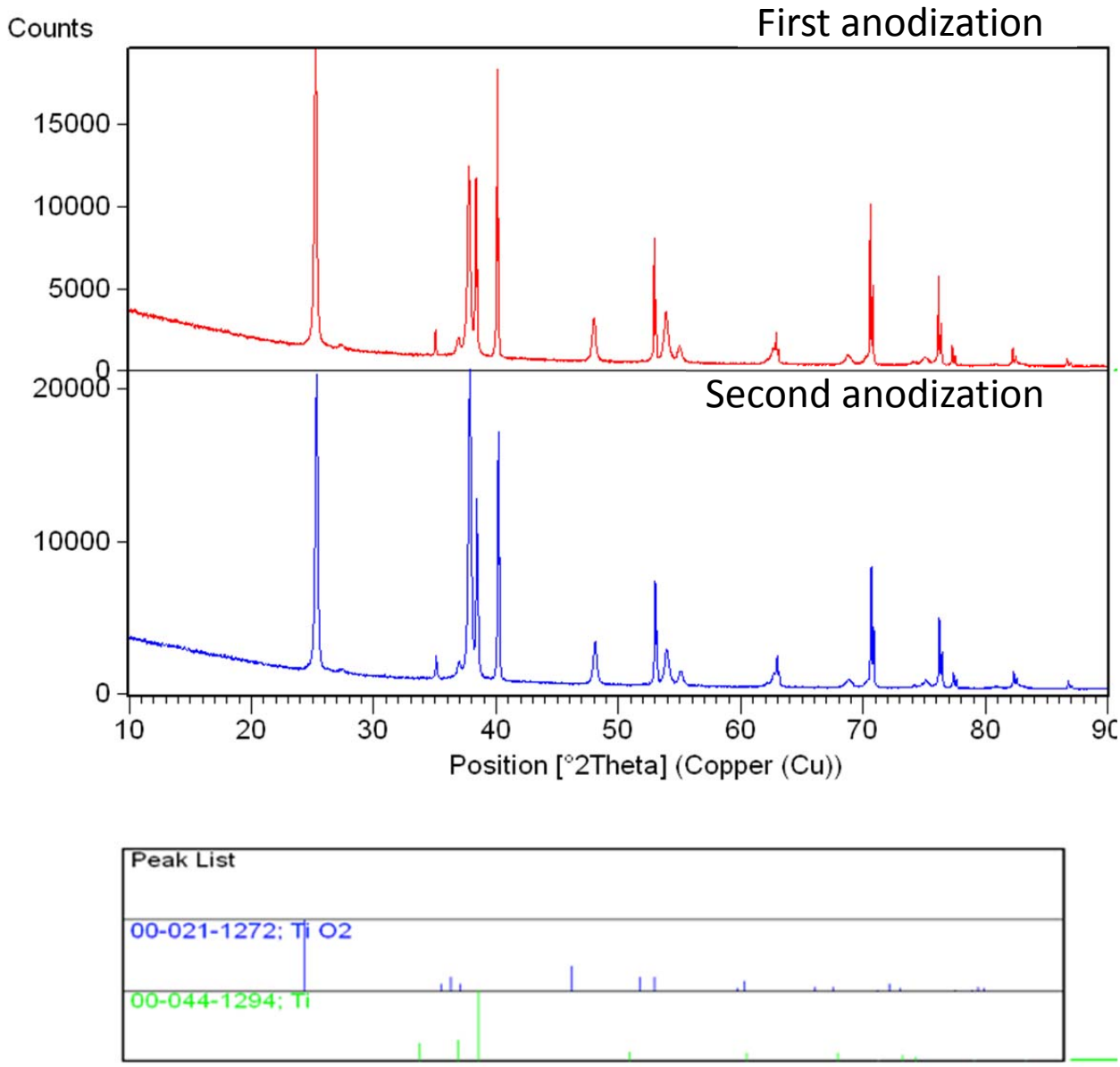


**Figure 3.** XRD patterns of $TiO_2$ NTs after the first and second anodization. The peak patterns for $TiO_2$ anatase (00-021-1272) and Ti (00-044-1294) are included below the graph as references.

### *3.1.2 $TiO_2$ NT membranes*

Several methods to detach the $TiO_2$ NTs from the Ti foil have been reported in the literature. One strategy is to use an anhydrous methanol/$Br_2$ solution to selectively dissolve the Ti substrate and leave the oxide layer [13]. Subsequent etching of the bottom of the membrane by HF will open the NTs but leave a slightly inhomogeneous bottom layer [14]. It is also possible to obtain a free-standing $TiO_2$ NT membrane by applying a large voltage pulse in-situ after the traditional anodization voltage is applied [15] [16]. Wang and Liu's separation procedure allows for control over the diameter of the NT openings on the bottom of the membrane [16]. In this work, the membrane was detached by creating an amorphous thin $TiO_2$ layer between the Ti foil and the anatase $TiO_2$ NTs. The sample was then exposed to 0.05 wt. % HF to selectively dissolve the amorphous layer, leaving a crystalline $TiO_2$ NT film. Figure 4 shows that the $TiO_2$ NTs preserved the same morphology after the detachment process. SEM images show that the membranes have excellent structural stability and the morphology is preserved during the detachment and transfer process.

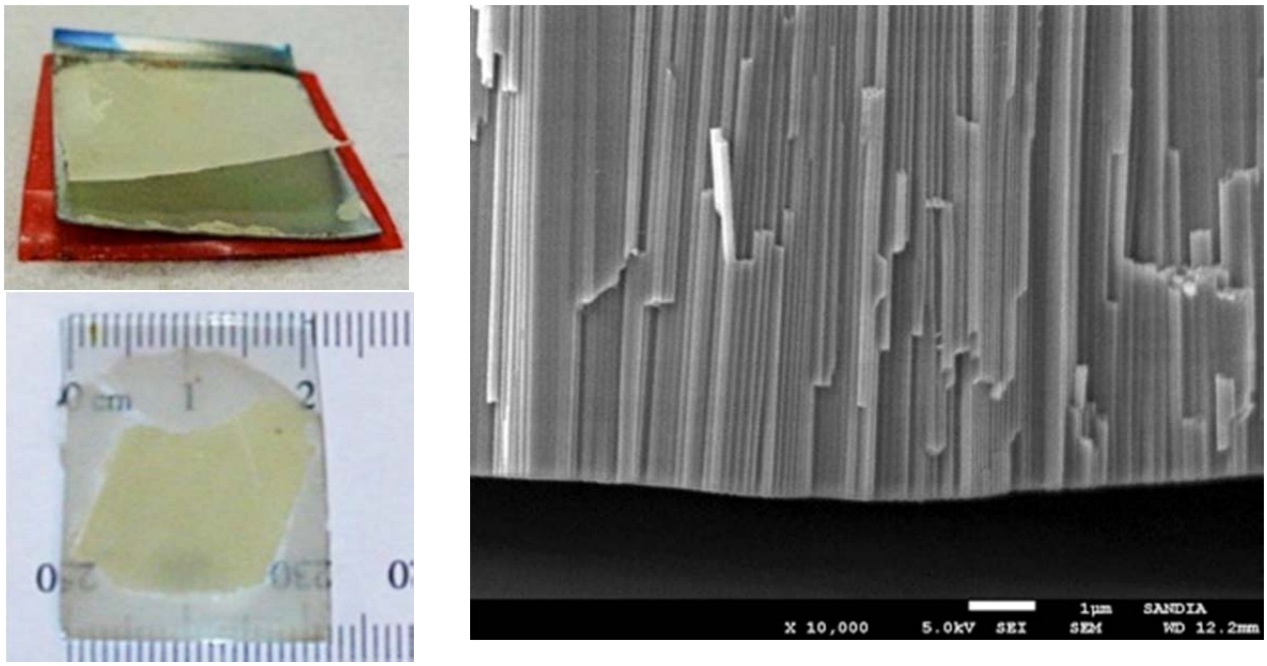


**Figure 4.** Photographs of $TiO_2$ NT membrane detached from the Ti foil and then transferred to FTO glass. SEM of the detached $TiO_2$ NTs from the Ti foil.

$TiO_2$ NT membranes with different thickness prepared using different anodization times (5 h, 2 h, 1 h, 50 min, 30 min, 20 min, and 10 min) were successfully detached. The dried membranes were relatively easy to handle with tweezers, and sizes bigger than 1 $cm^2$ can be detached and successfully transferred to the glass. However, the membranes prepared with anodization times less than 30 min were very thin and fragile and consequently very hard to transfer.

**Table 1.** Summary of techniques used to attach $TiO_2$ NT membranes.

| Label | Attachment Technique | Membrane Area ($cm^2$) |
|---|---|---|
| 1 | $TiO_2$ paste with 2 drops $Ti(OBu)_4$ and 4 drops PEG. After it was transferred it was dried in ambient air for 2 h before annealing. Pressure was applied during annealing. | Detached |
| 2 | 2 drops $Ti(OBu)_4$ and 4 drops PEG. Pressure was applied during annealing. | Detached |
| 3 | P25 $TiO_2$ paste. Pressure was applied during annealing. | 1.3 |
| 4 | 2 drops $Ti(OBu)_4$ with applied pressure during annealing. | Detached |
| 1A | $TiO_2$ paste with 2 drops $Ti(OBu)_4$ and 4 drops PEG. | Detached |
| 2A | $TiO_2$ paste with 2 drops $Ti(OBu)_4$ and 4 drops PEG. Pressure was applied during annealing. | 1.4 |
| 3A | $TiO_2$ paste with 2 drops $Ti(OBu)_4$ and 2 drops PEG. Pressure was applied during annealing. | Detached |
| 4A | $TiO_2$ paste with 3 drops $Ti(OBu)_4$ and 4 drops PEG. Pressure was applied during annealing. | Detached |
| 5A | $TiO_2$ paste with 4 drops $Ti(OBu)_4$ and 4 drops PEG. Pressure was applied during annealing. | Detached |
| 6A | $TiO_2$ paste with 2 drops $Ti(OBu)_4$ and 3 drops PEG. Pressure was applied during annealing. | Detached |
| 7A | 1-2 drops aged 0.1 M Ti-isoproproxide in 2-propanol. | 1.5 |
| 8A | 1-2 drops fresh 0.1 M Ti-isoproproxide in 2-propanol. | 0.5 |
| 9A | 1-2 drops aged 0.1 M Ti-isoproproxide in 2-propanol. Pressure was applied during annealing. | 0.9 |
| 10A | 1-2 drops fresh 0.1 M Ti-isoproproxide in 2-propanol. Pressure was applied during annealing. | 1.3 |
| 1B | 1-2 drops fresh 0.1 M Ti-isoproproxide in 2-propanol. Pressure was applied during annealing. | 3.1 |
| 2B | 1-2 drops fresh 0.1 M Ti-isoproproxide in 2-propanol. Pressure was applied during annealing. | 1.0 |
| 3B | 1-2 drops aged 0.1 M Ti-isoproproxide in 2-propanol. Pressure was applied during annealing. | 0.5 |
| 4B | 1-2 drops aged 0.1 M Ti-isoproproxide in 2-propanol. | 1.0 |

Table 1 summarizes several techniques used to attach the membrane to the glass. The samples were analyzed by cyclic voltammetry (CV) in order to examine the different attachment techniques. A successful attachment is one that reproducibly shows high conductivity, indicated by high current in the CV, and reversibility, indicated by a ratio of the peak anodic current to the peak cathodic current near 1:1 [17]. Perchloric acid is used as the electrolyte because the film is stable under acidic conditions, the perchlorate ion interacts minimally with the film, and H+ is an effective intercalating ion that is likely to bind to oxygen atoms when the film is in a partially reduced state. As shown in Figure 5 (a), $TiO_2$ NTs on Ti foil shows a very high conductivity and reversibility. All samples in Figure 5 (b and c) show that the interface used to attach the $TiO_2$

NTs to the FTO glass reduced the conductivity and caused the intercalation redox event to be partially irreversible. Samples 3 and 7A show better reversibility and a higher current density in Figure 5(b). Several more samples were prepared using these two techniques. The results indicate that the reproducibility of the attachment technique for Sample 7A was poor. However, the results for multiple samples using the Sample 3 technique showed that the P25 paste creates an interface for the $TiO_2$ NT film to attach to the FTO glass that retains the NTs conductivity, does not cause an irreversible redox reaction, and is reproducible. Due to the success of this attachment technique, further experiments mentioned in this report are attached using this method.

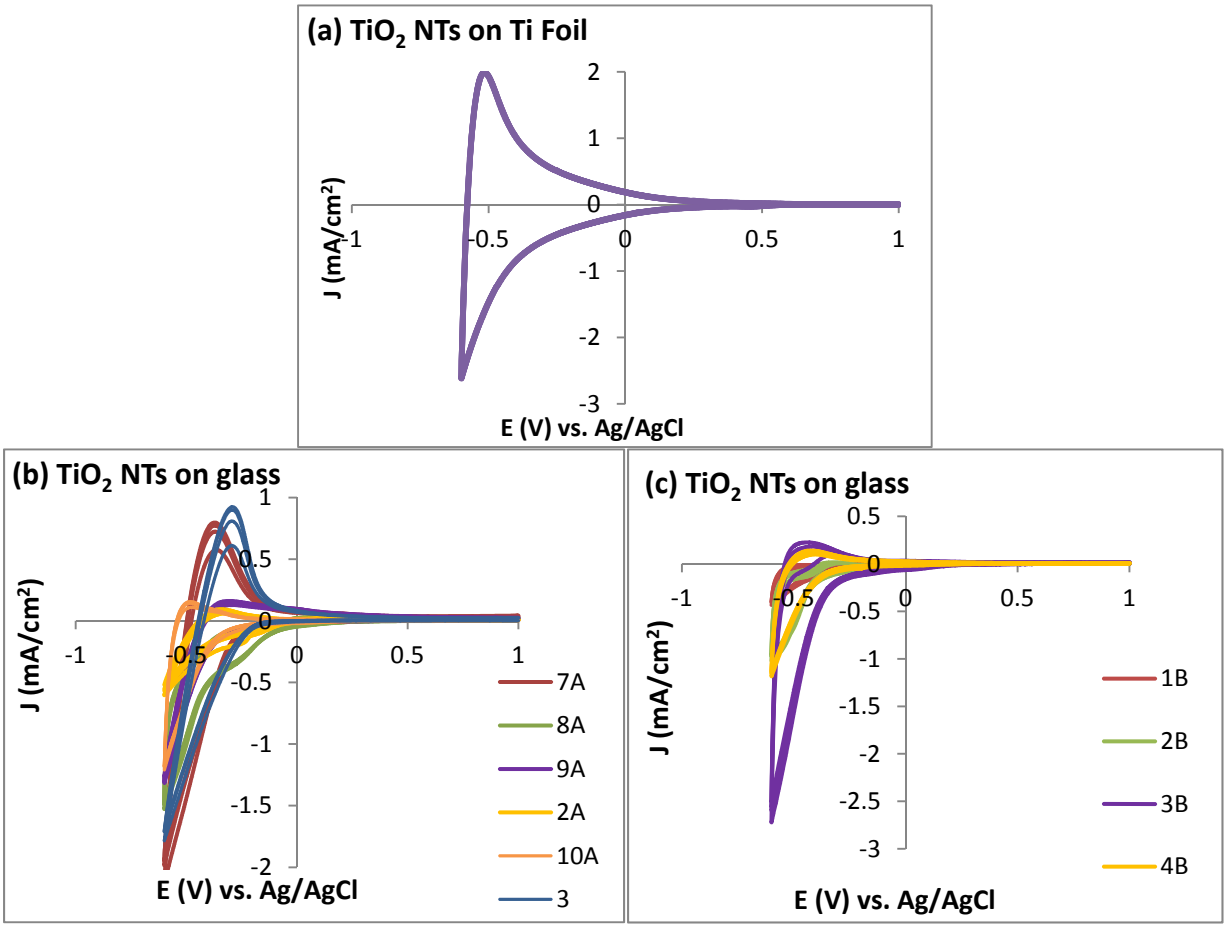


**Figure 5.** CV of (a) $TiO_2$ NTs on Ti foil and (b and c) $TiO_2$ NTs on glass between 1 V to -0.6 V at 40 mV $s^{-1}$ in 0.1 M $HClO_4$. The details for the attachment tecniques for each sample are described in Table 1.

### *3.1.3 $WO_3$ electrodeposition*

High quality $WO_3$ films are most generally obtained by vacuum evaporation and sputtering. Unfortunately, these methods are time consuming and very expensive. Wet low-cost methods, such as electrodeposition, seem to be very promising approach to create $WO_3$ films. The film

electrodeposition method is based on the cathodic reduction of a peroxo precursor, which is obtained by mixing a tungsten precursor with hydrogen peroxide. The most generally precursor used is tungsten metal, but unfortunately this precursor solution is highly unstable. Independently of the route used to obtain the deposition solution, the precursor is always prepared in an excess of hydrogen peroxide and described as a dimer with the formulae $W_2O_{11}^{2-}$ with ($O_2$) a peroxide ligand. The oxidation state of W is +VI. The deposition reaction is described as:

$$W_2O_{11}^{2-} + (2 + x)H^+ + xe^- \rightarrow 2\ WO_3 + (2 + x)/2H_2O + (8 - x)/4O_2$$

It has been shown that parallel parasitic reactions take place and should correspond to hydrogen evolution, colloidal $WO_3$ formation and reduction of free $H_2O_2$, residual $O_2$ and polytungstate. Due to all the parasitic reactions and uncertainty of the deposition efficiency and stoichiometry, we decided to report deposited amounts in deposited charge density (mAh) instead of moles.

To the best of our knowledge, this work is the first one to use $TiO_2$ nanotubes as substrates for $WO_3$ electrodeposition. Annealed $TiO_2$ NTs membranes on Ti foil or FTO glass were used as substrate for $WO_3$ electrodeposition. $TiO_2$ NTs have to be annealed before the electrodeposition because amorphous $TiO_2$ partially dissolves in tungstic acid solution.

## 3.2 Characterization of composite materials

### *3.2.1 X-ray diffraction*

Figure 6 shows the X-ray diffraction (XRD) patterns of $TiO_2$, $WO_3$ and $WO_3/TiO_2$ composite films, all of which had been annealed in air for 2 h. $TiO_2$ NTs show the distinct peaks for anatase phase. No other XRD peaks except for substrate (FTO) peaks were detected indicating a single compound. XRD patterns of $TiO_2$ NT on Ti foil collected before the detachment/transfer to the glass show the same anatase phase, indicating that the crystal structure is not affected by the detachment/transfer process.

The $WO_3$ film showed three distinct peaks in the range $23^o < 2\theta < 25^o$. These three peaks can be observed in the $WO_3$ electrodeposited on FTO glass as well as on Ti foil. $WO_3$, given its simple stoichiometry, can be found in large variety of crystal structures (e.g., monoclinic, orthorhombic, and triclinic). Comparing the XRD patterns with the JCPD reference files, the diffraction peaks resemble those of a monoclinic structure (JCPD # 43-1035), the most stable phase at room temperature and a photoactive phase of $WO_3$.

For the composite materials, a predominant peak with a broad shoulder is observed. The predominant peak ($2\theta = 25^o$) can be assigned to $TiO_2$ anatase phase and the broad shoulder ($23^o < 2\theta < 25^o$) to the three $WO_3$ monoclinic peaks. No additional peaks were detected, indicating the absence of Ti-W alloys. Figure 7 shows that composite materials prepared with $TiO_2$ NTs with different anodization times (different lengths) have very similar XRD patterns.

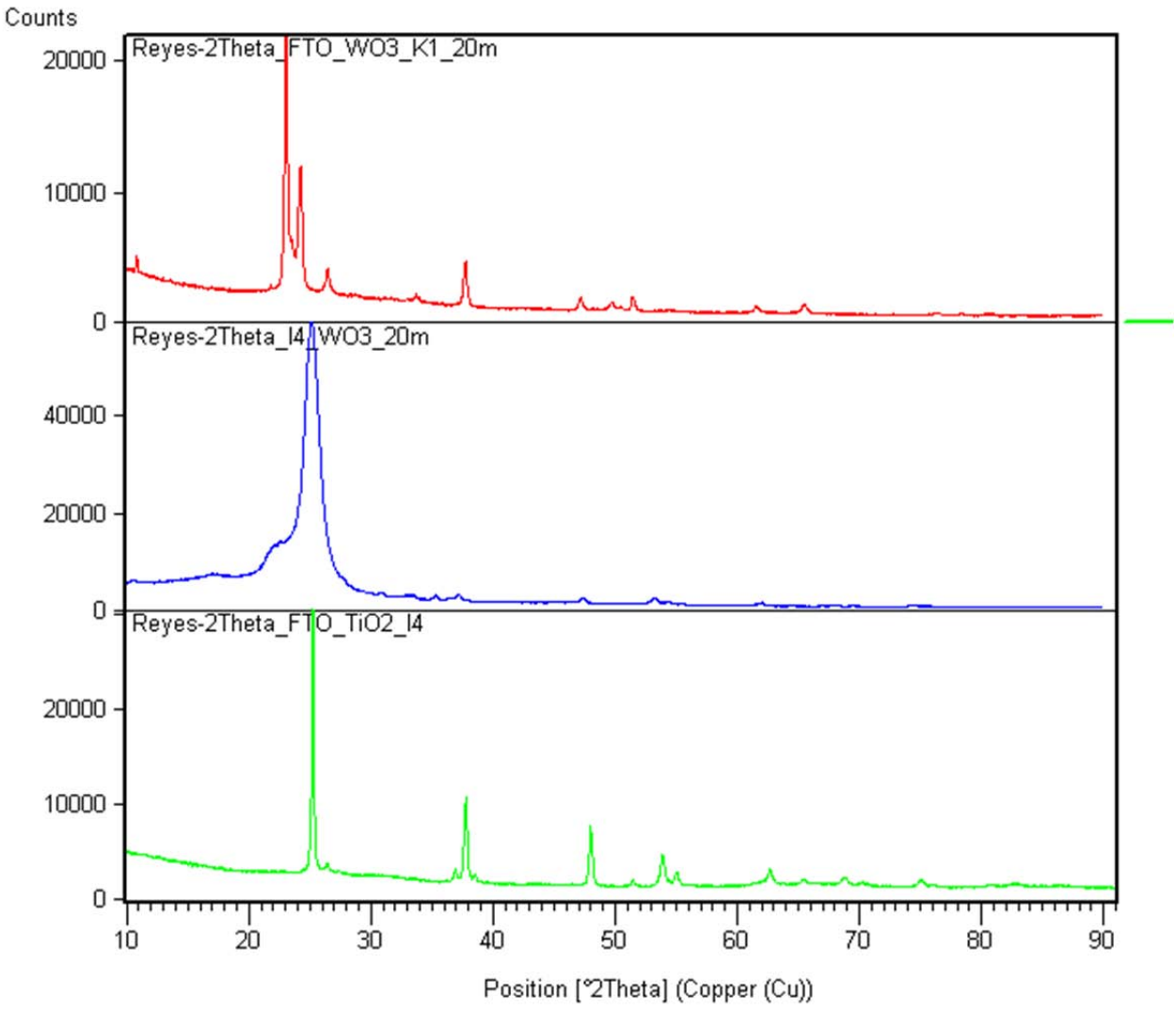


**Figure 6.** XRD of $WO_3$ (red line), $WO_3$/ $TiO_2$ NT (blue) and $TiO_2$ NT (green) on FTO glass.

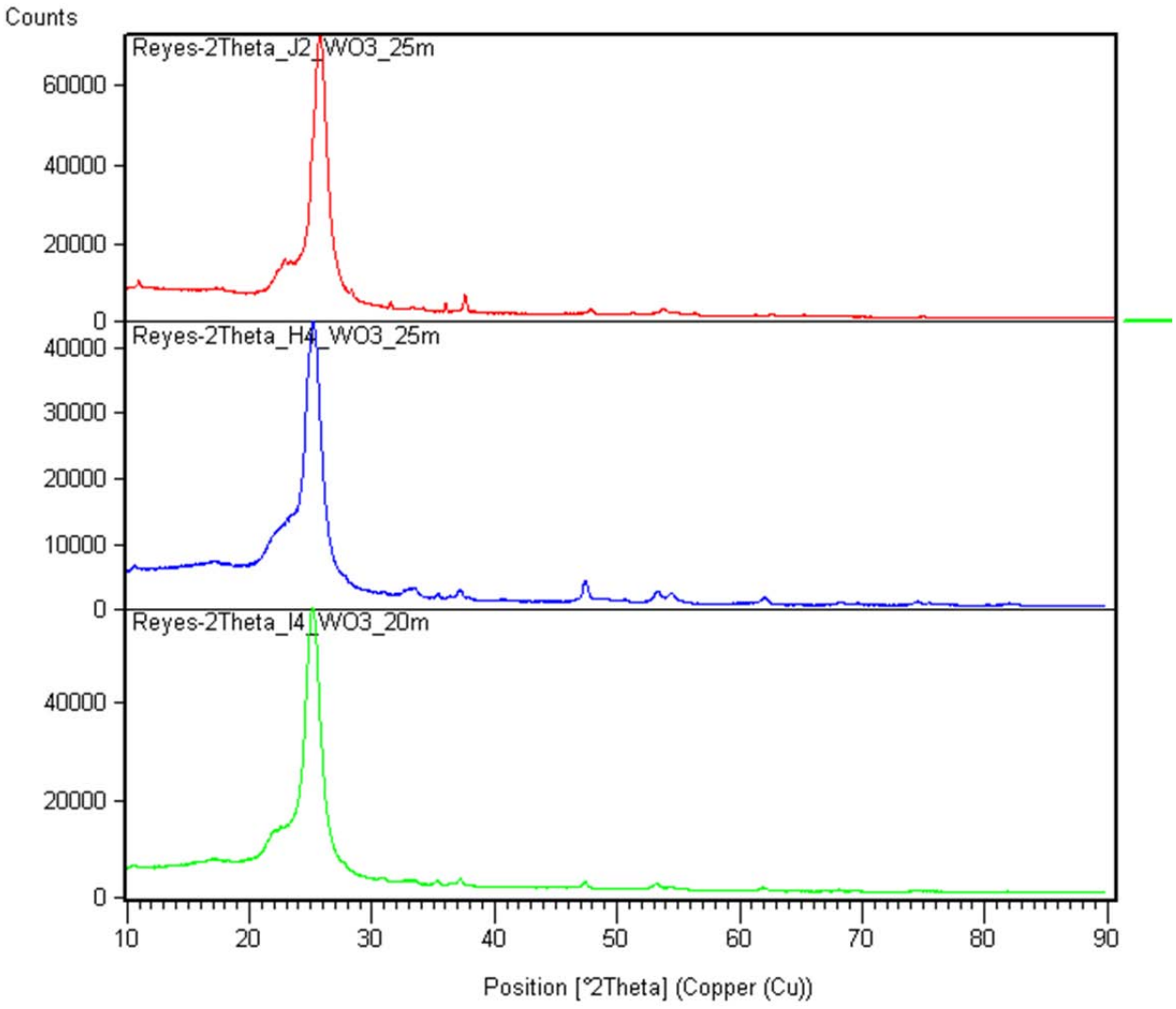


**Figure 7.** XRD of $WO_3$/ $TiO_2$ NTs using $TiO_2$ NT substrates with different anodization times: 1 h (red line), 2 h (blue line), and 5 h (green line).

### *3.2.2 Scanning electron microscope images*

Figures 8 and 9 show the SEM plain-view images of composite materials on FTO glass. Diverse $WO_3$ nanostructures can be seen in the same sample, including nanorods, coral-shaped structures, and nanofibers. When $WO_3$ is electrodeposited on flat surfaces (such as glass), the resulted $WO_3$ film is a compact film with no defined structure. However, in this study we show that $TiO_2$ nanotubes act a skeleton to create defined nanostructures.

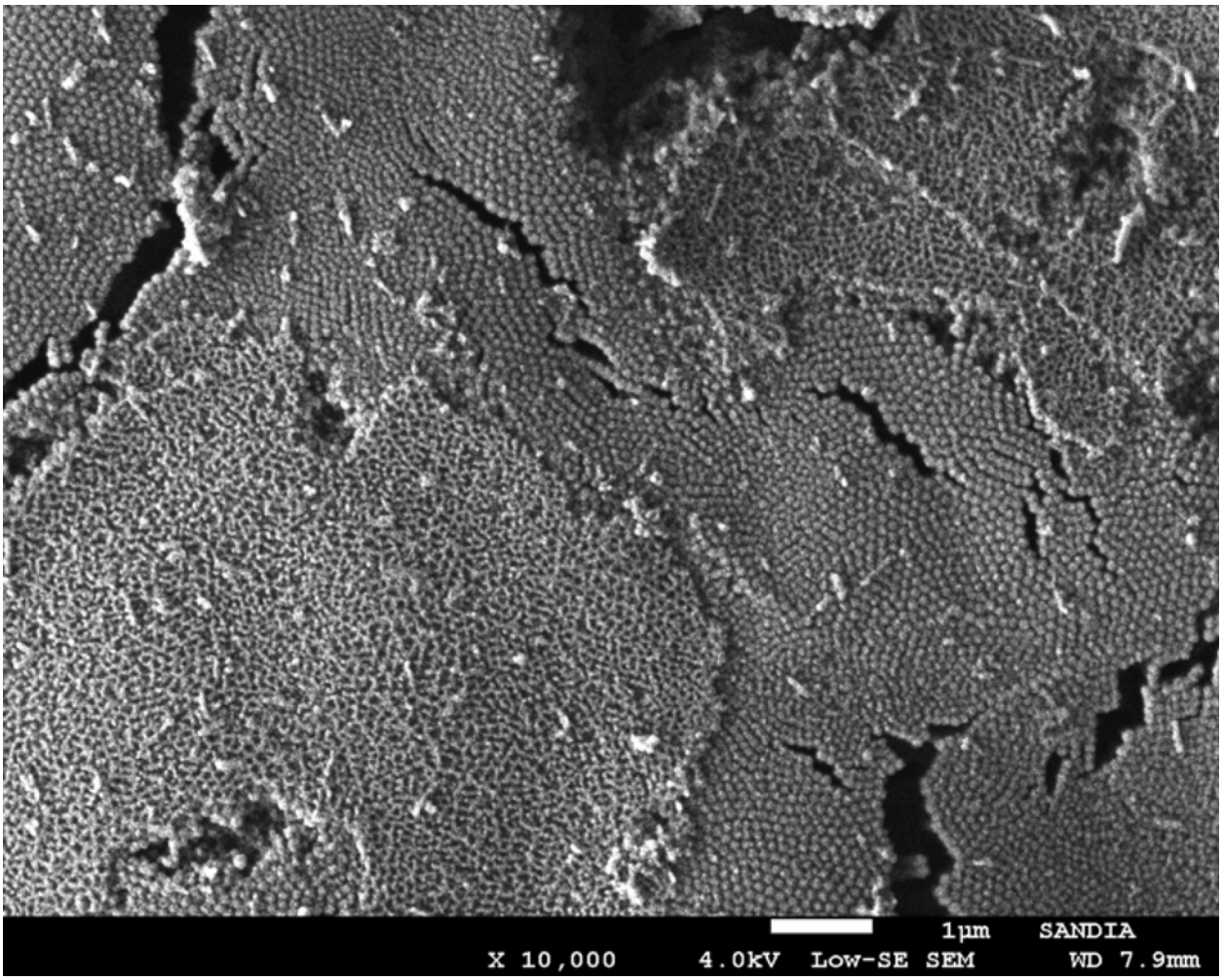


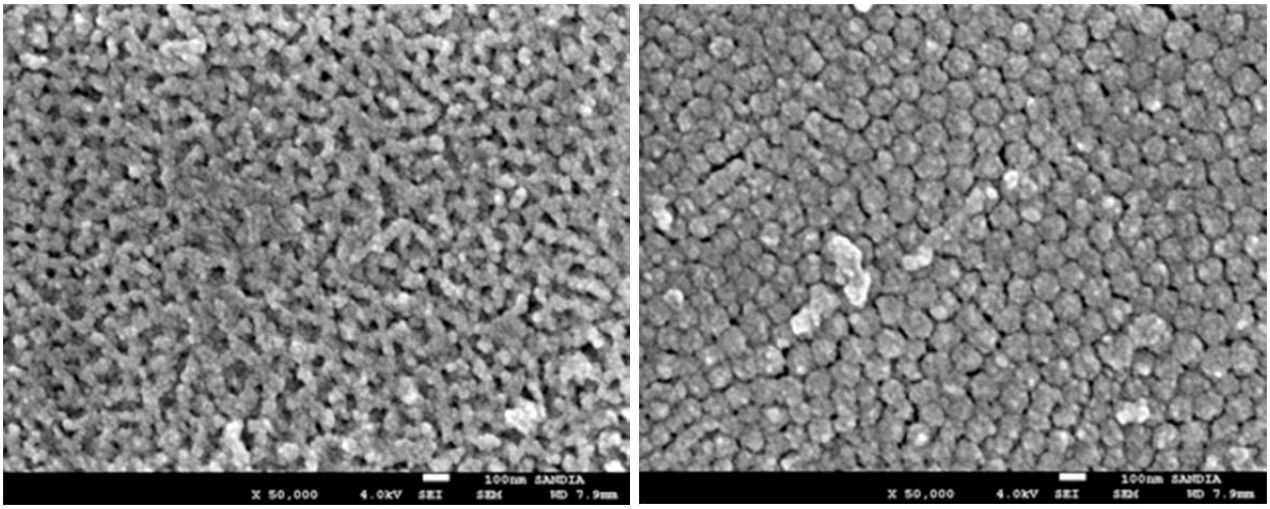

**Figure 8.** SEM plan-view images of $WO_3/TiO_2$ NT membrane (J3) on FTO glass. The anodization time for the $TiO_2$ NT substrate was 1 h.

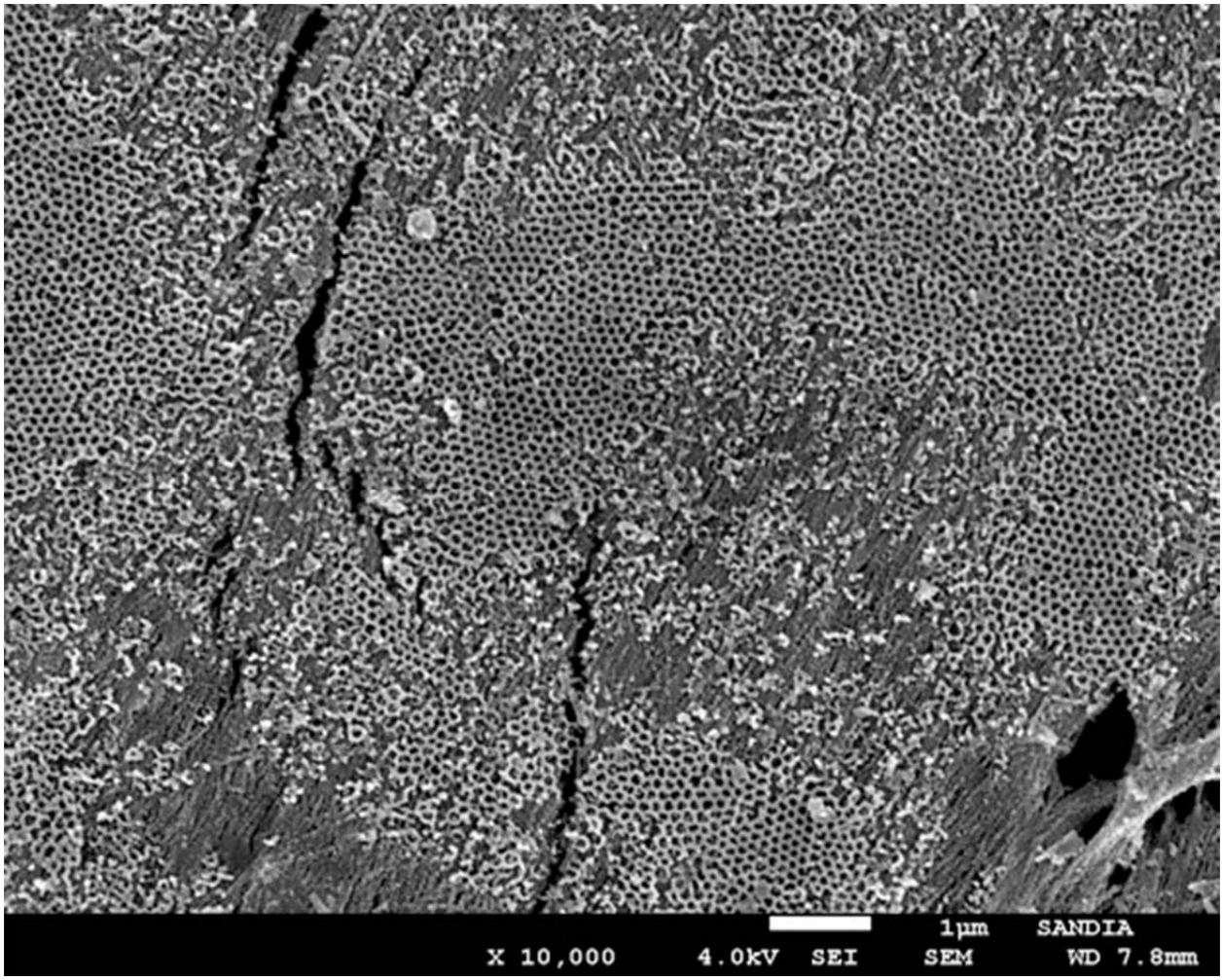


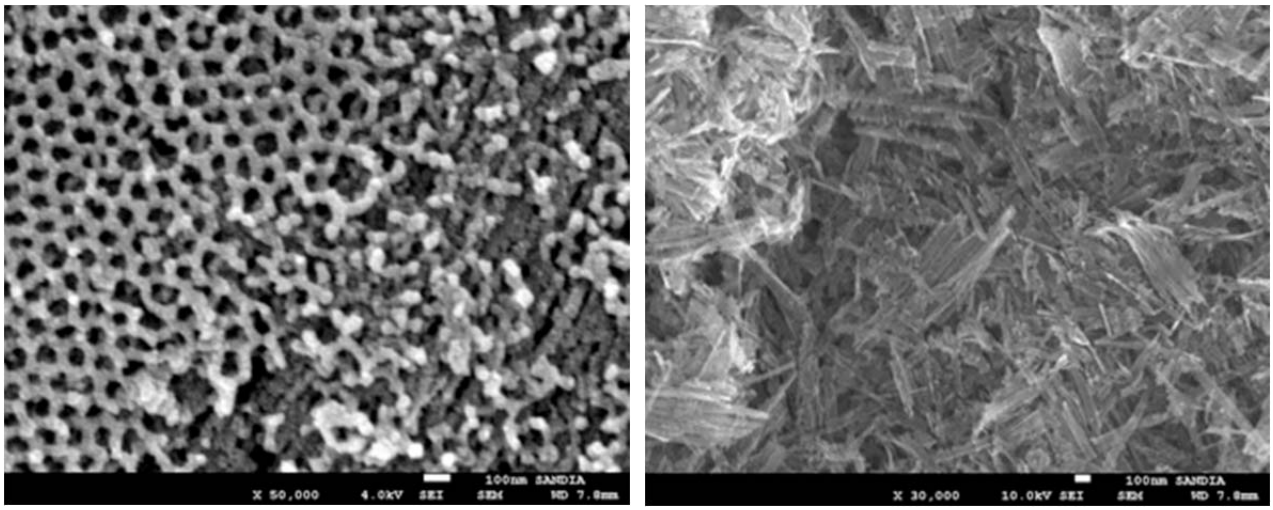

**Figure 9.** SEM plan-view images of $WO_3/TiO_2$ NT membrane (I1) on FTO glass. The anodization time for $TiO_2$ NT substrate was 5 h.

To obtain the cross sectional images, the membranes on the FTO glass were fractured using a diamond pen and mounted at 90 degrees. As shown in the SEM images (Figure 10) and Table 2, the length of the $TiO_2$ nanotubes is directly proportional to the anodization time. The thickness of the P25 paste used as the adhesion layer ranges between 14-37 µm and depends on the application technique. The nanotubes look very well vertically organized and the P25 layers appear to form a nanoparticle network. The SEM images show good connectivity between the nanotubes and the P25 layer. Some fractured nanotubes and debris can be seen as result of the fracture process.

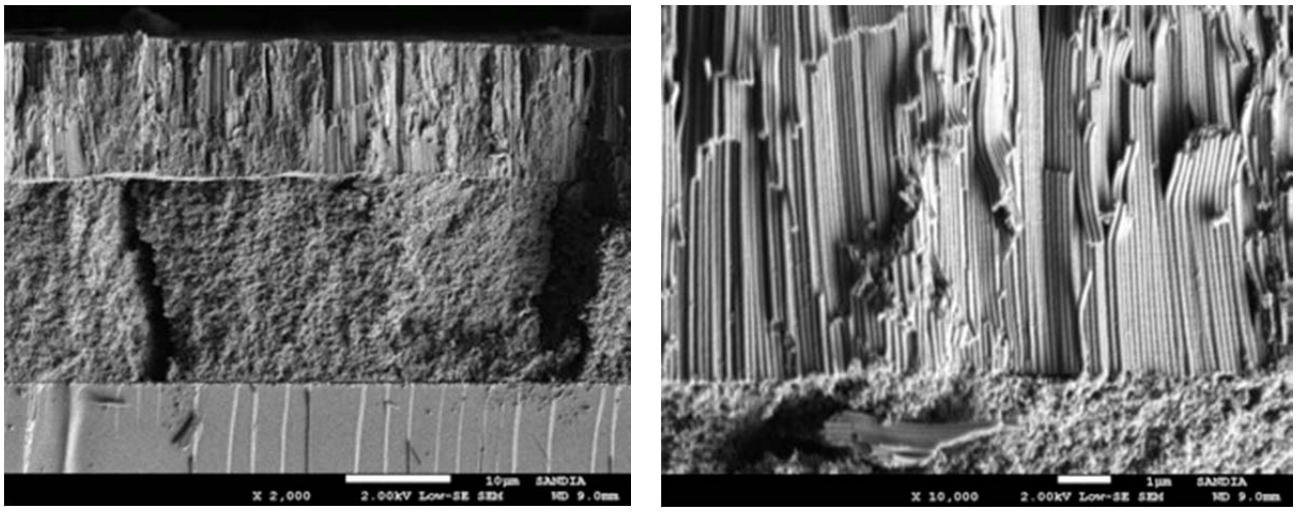


**Figure 10.** SEM cross sectional images of $TiO_2$ NT membrane (H5) on P25 layer/FTO glass. Anodization time was 2 h and the estimated thickness of the $TiO_2$ NTs was 12.8 µm.

**Table 2.** $TiO_2$ nanotube length and P25 thickness calculated from SEM cross sectional images.

| Sample labels | Anodization time (time) | $WO_3$ | $TiO_2$ NT length (µm) | P25 thickness (µm) |
|---|---|---|---|---|
| J1 | 1 h | | 5.79 ± 0.03 | 14.1 ± 0.8 |
| J3 | 1 h | Yes | 6.4 ± 0.7 | 25 ± 1 |
| H5 | 2 h | | 12.8 ± 0.6 | 17 ± 3 |
| H4 | 2 h | Yes | 11.9 ± 0.3 | 37 ± 1 |
| I6 | 5 h | | 15.8 ± 0.4 | 16.2 ± 0.6 |
| I1 | 5 h | Yes | 22.2 ± 0.8 | 24 ± 2 |

### *3.2.3 Energy-dispersive X-ray spectroscopy*

EDS was performed in at least five different areas in the same sample in order to accurately represent the whole sample. Figure 11 shows two representative spectra for bare $TiO_2$ NTs and $WO_3/TiO_2$ NTs. The main elements found in $TiO_2$ NTs were titanium and oxygen. Trace amount of gold were detected because gold was sputtered on the sample to avoid charging. Tungsten peaks were almost undetectable, indicating either the absence of $WO_3$ or presence at only a trace

level (probably due to contamination). However, for the $WO_3/TiO_2$ NTs, the tungsten peaks were predominant and very well defined. The average atomic percentages for the main elements detected by EDS are summarized in Table 3.

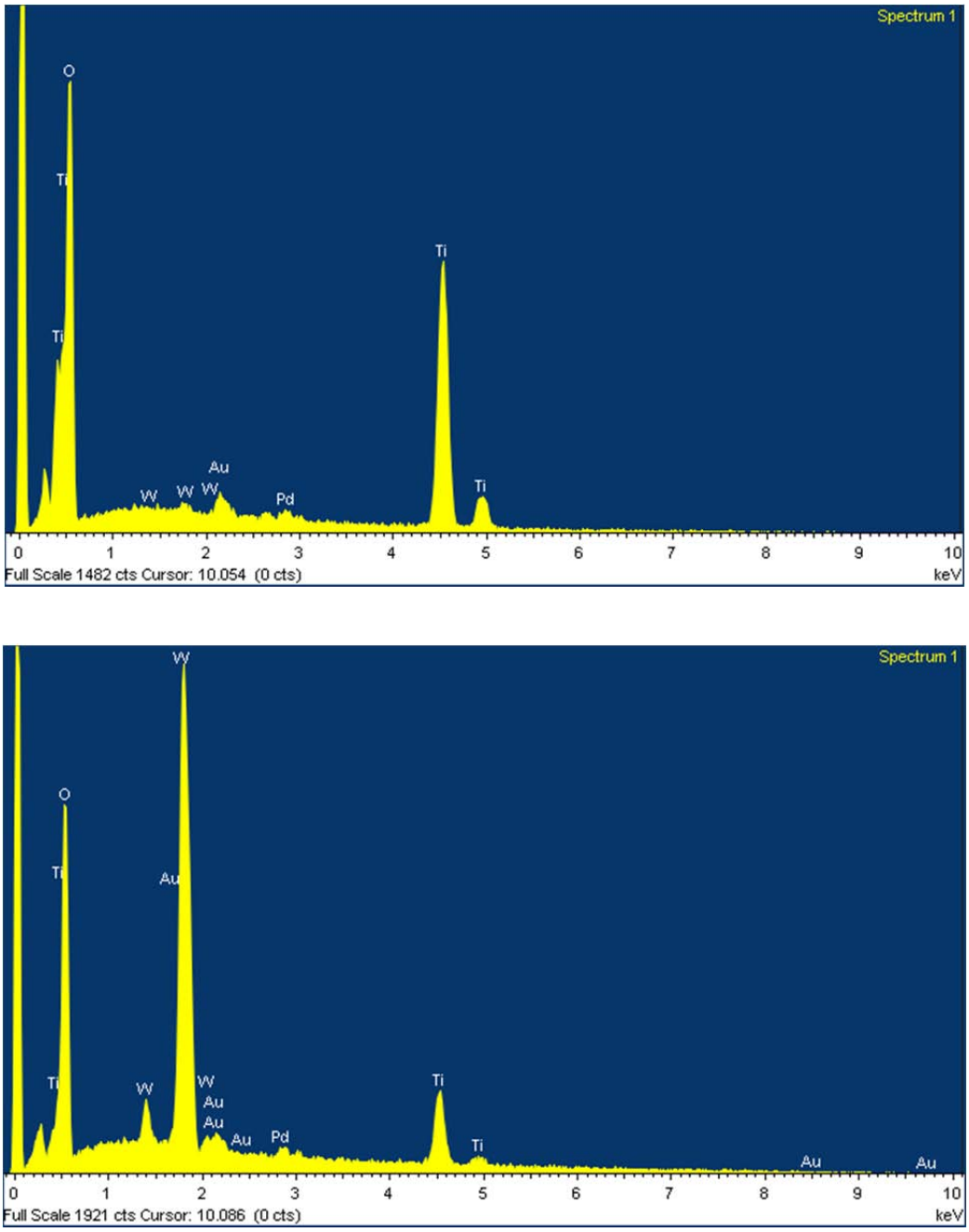


**Figure 11.** EDS spectra of $TiO_2$ NTs (top) and $WO_3/TiO_2$ NTs (bottom) on glass.

**Table 3.** Average atomic percentages (at %) of the main elements found in the EDS spectra.

| Sample labels | Ti anodization time (time) | $WO_3$ | O (at %) | Ti (at %) | W (at %) |
|---|---|---|---|---|---|
| H5 | 2 h | No | 72 ± 2 | 28 ± 2 | 0 |
| J3 | 1 h | Yes | 72 ± 1 | 25 ± 1 | 2.9 ± 0.4 |
| H4 | 2 h | Yes | 73 ± 1 | 15 ± 1 | 12 ± 1 |
| I1 | 5 h | Yes | 71 ± 1 | 23 ± 1 | 6.6 ± 0.1 |

## 3.3 Electrochromic testing

### *3.3.1 Cyclic voltammetry-ion storage capacity*

Figure 12 shows the CVs for the $TiO_2$ NT membranes on FTO glass. $TiO_2$ NTs with different lengths showed similar CVs, indicating that the nanotubes length does not significantly affect the current density of $TiO_2$. This may be because only the outer surface of the tubes contributes to the current. The ion capacity of the material during the redox reaction, or the anodic and cathodic charge, can be found by integrating the current density versus time curve. The charge capacities for the best $TiO_2$ NT membranes at each anodization time are listed in Table 4. The ratio of anodic and cathodic charge indicates how reversible the redox process is. A ratio of 1 indicates a completely reversible process. The $TiO_2$ NTs on FTO glass obtained a ratio of ~0.8, indicating that the process is partly reversible. We expect that an ion intercalation process will be highly reversible, with a high ratio that is stable over multiple cycles, an issue discussed below. If ions intercalate irreversibly, we will see a decrease in current density with each cycle. If there is no such decrease, the irreversible process is more likely to be due to a redox process where the products diffuse away, such as water reduction to form $H_2$.

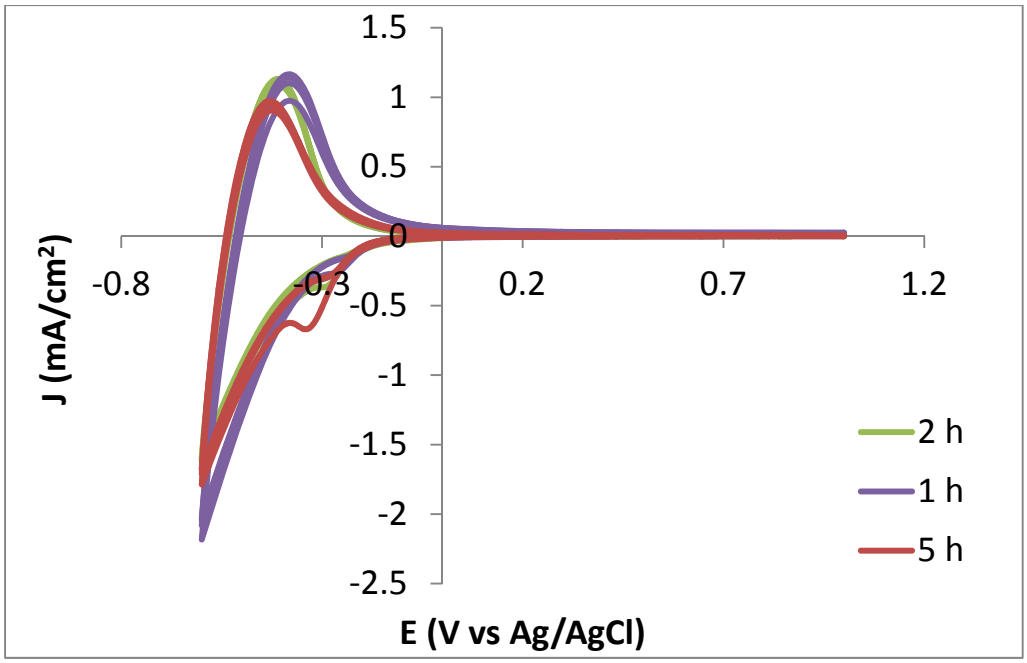


**Figure 12.** CV of $TiO_2$ NT film formed by anodization at different times attached to FTO glass with $TiO_2$ P25 paste in 0.1 M $HClO_4$ electrolyte solution at a scan rate of 40 mV $s^{-1}$.

**Table 4.** The charge capacity of $TiO_2$ NTs on FTO glass before $WO_3$ electrodeposition. Data calculated from CV in 0.1 M $HClO_4$ electrolyte solution at a scan rate of 40 mV $s^{-1}$.

| Membrane | Ti anodization time (h) | Area ($cm^2$) | $Q_{anodic}$ (mC $cm^{-2}$) | $Q_{cathodic}$ (mC $cm^{-2}$) | $Q_{anodic}/Q_{cathodic}$ |
|---|---|---|---|---|---|
| J2 | 1 | 0.699 | 10.200 | -12.564 | 0.812 |
| M4 | 1 | 1.140 | 5.971 | -7.437 | 0.803 |
| L1 | 2 | 0.268 | 5.981 | -8.082 | 0.740 |
| L4 | 2 | 0.352 | 8.099 | -10.318 | 0.785 |
| I1 | 5 | 0.982 | 4.726 | -5.587 | 0.846 |
| H1 | 5 | 0.508 | 7.611 | -9.955 | 0.765 |

### *3.3.2 Effect of $WO_3$ deposited charge density*

To study how the $WO_3$ concentration affects the electrochromic performance, different concentrations were electrodeposited on FTO glass and analyzed by CV. Figure 13 indicates that the current density increases with increasing $WO_3$ concentration, with about a 0.1 mA $cm^{-2}$ increase in current density when the $WO_3$ deposited charge density increases from 0.225 to 0.3375 mA h $cm^{-2}$. The CV current density vs. deposited charge density slope is less than 1,

suggesting either a deposition efficiency that decreases with thickness, or that deeper regions in the deposited film contribute less current to the CV.

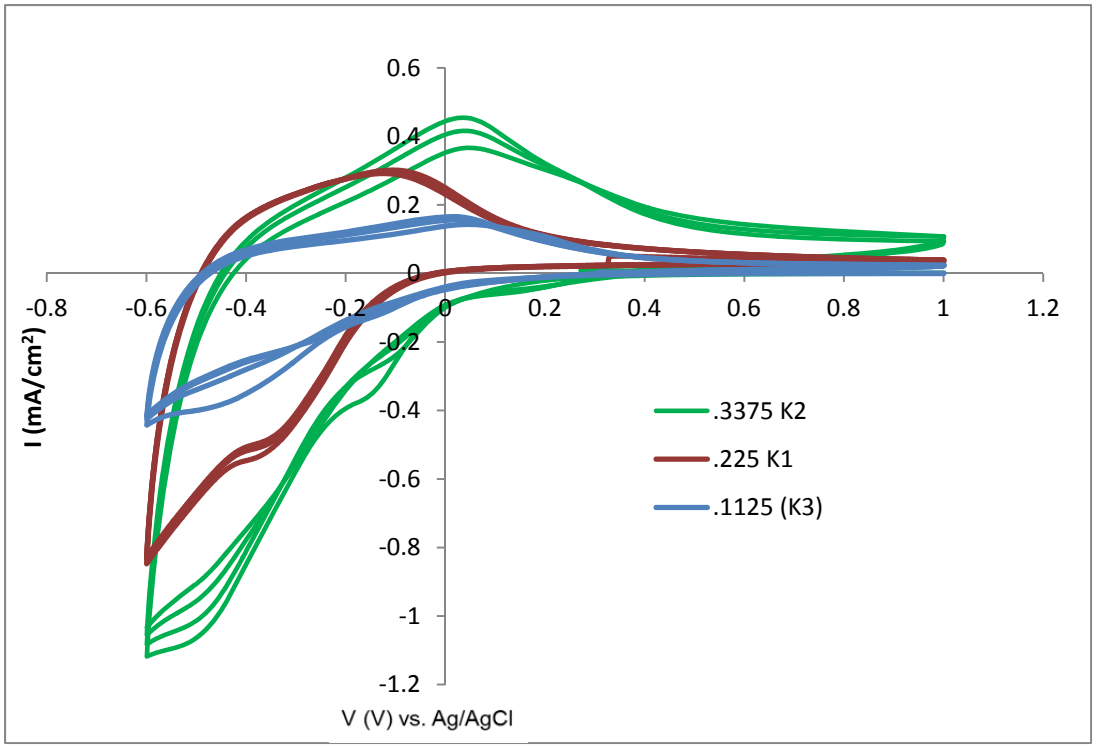


**Figure 13.** Cyclic voltammograms of different deposited charge densities of $WO_3$ (0.3375, 0.225, and 0.1125 mA h $cm^{-2}$) electrodeposited on FTO glass in 0.1 M $HClO_4$ electrolyte solution at a scan rate of 40 mV $s^{-1}$.

Initially, the composite materials were prepared on the Ti foil, and then the CV results were compared with the $WO_3$/FTO and $TiO_2$ NTs on Ti foil. As shown in Figure 14, the composite $WO_3/TiO_2$ NT electrodes showed a significant enhancement in ion storage capacity compared to the single materials: $TiO_2$ nanotubes and $WO_3$ nanoparticles, indicating that the underlying $TiO_2$ NTs and the $TiO_2/WO_3$ interface are sufficiently conductive to allow electrochemical switching of the $WO_3$ external layer. Benoit et al. reported the "decoration" of $TiO_2$ nanotubes with $WO_3$ nanocrystals by the hydrolysis of a $WCl_6$ [8]. The authors also found that the decorated nanotubes show a remarkable enhancement of the electrochemical properties. However, their best material only reached current density of 1.25 mA/$cm^2$ under similar experimental conditions (scan rate of 50 mV/s in 0.1 M $HClO_4$ electrolyte and a voltage range of -0.5V and 1V) However, our best material reached current density of 10 mA/$cm^2$. We believe that this is the highest reported current density to date for $TiO_2$, $WO_3$ and $TiO_2$-$WO_3$ composite materials.

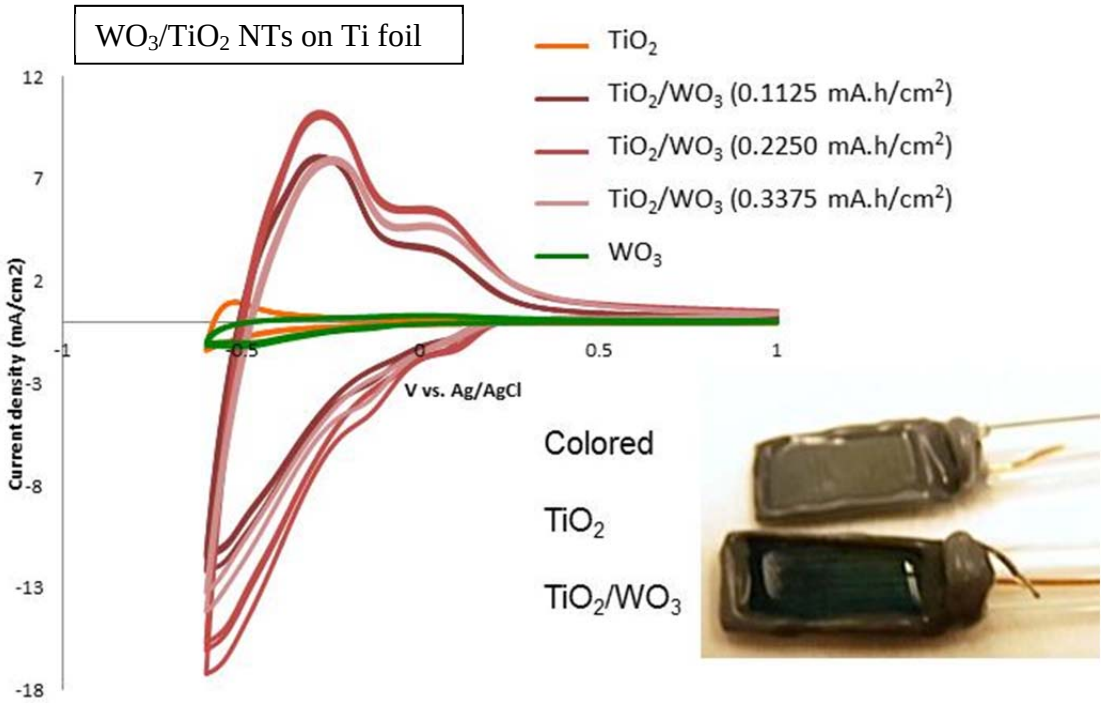


**Figure 14.** CV of $WO_3$/ $TiO_2$ NTs on Ti foil in 0.1 M $HClO_4$ electrolyte solution at a scan rate of 40 mV $s^{-1}$. The photograph shows the colored electrodes.

According to Figure 14, $WO_3/TiO_2$ NTs (0.2250 mA.h/$cm^2$) on Ti foil showed the highest current densities. $WO_3/TiO_2$ NTs with different $WO_3$ concentrations (0.2250 and 0.3375 mA.h/$cm^2$) and different anodization times (1, 2, and 5 h) were detached from the Ti foil and transferred to FTO. Figure 15 shows that the $WO_3/TiO_2$ NT membranes on FTO have slightly lower current densities and similar reversibility to those of $WO_3/TiO_2$ NTs on Ti foil (Figure 14). These results suggest that the detachment/transfer techniques successfully retain the good charge transport capabilities with no significant negative effects on either ion storage capacity or redox reversibility.

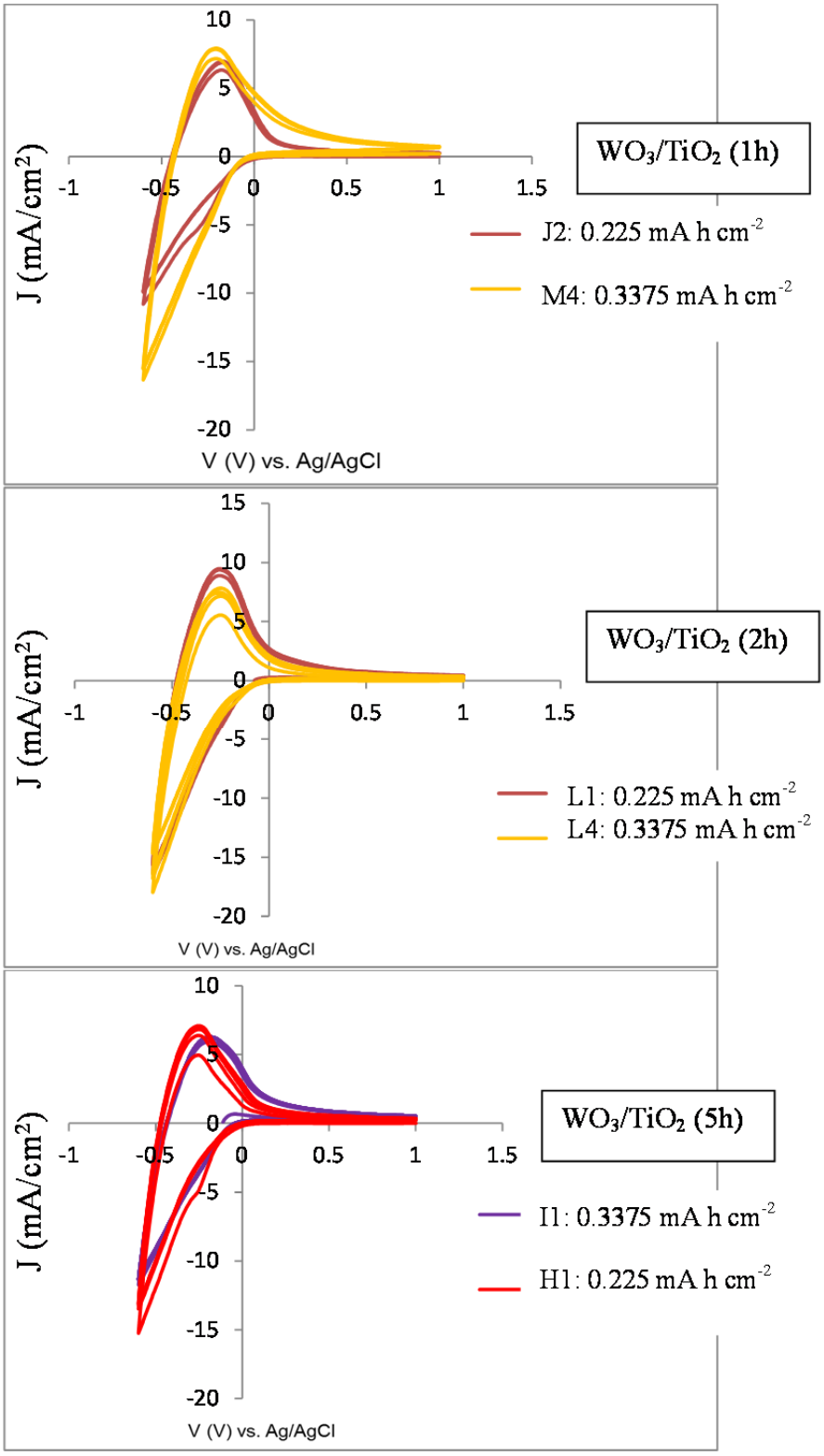


**Figure 15.** CV for $WO_3/TiO_2$ membranes on FTO glass with different Ti anodization times (1 h, 2 h, and 5 h) and different $WO_3$ concentrations (0.225 and 0.3375 mA h $cm^{-2}$) in 0.1 M $HClO_4$ electrolyte solution at a scan rate of 40 mV $s^{-1}$.

Comparing the results for bare $TiO_2$ NT membranes before (Table 4) and after $WO_3$ electrodeposition (Table 5), it can been seen that when $WO_3$ is electrodeposited on $TiO_2$ NT membranes not only the charge carrying capacity of the material increases, but also the reversibility of the redox reaction increases with the $WO_3$. The charge capacity is approximately 10 times higher and the charge ratio increases from ~0.8 to ~0.9 (as high as 0.97 for some samples). Figure 15 indicates that increasing the $WO_3$ deposited charge density on the $TiO_2$ NT films contributes a negligible amount to the CV current density.

**Table 5.** The charge capacity of $TiO_2$ NTs on FTO glass after $WO_3$ electrodeposition. Data calculated from CV in 0.1 M $HClO_4$ electrolyte solution at a scan rate of 40 mV $s^{-1}$.

| Sample | Ti anodization Time (h) | $WO_3$ electrodeposition(m A h $cm^{-2}$) | Area ($cm^2$) | $Q_{anodic}$ (mC $cm^{-2}$) | $Q_{cathodic}$ (mC $cm^{-2}$) | $Q_{anodic}$/ $Q_{cathodic}$ |
|---|---|---|---|---|---|---|
| J2 | 1 | 0.225 | 0.28 | 75.06 | -79.32 | 0.95 |
| L1 | 2 | 0.225 | 0.08 | 98.22 | -110.45 | 0.89 |
| I1 | 5 | 0.225 | 0.10 | 83.10 | -90.83 | 0.91 |
| M4 | 1 | 0.3375 | 0.34 | 117.98 | -124.40 | 0.95 |
| L4 | 2 | 0.3375 | 0.10 | 81.67 | -93.94 | 0.87 |
| H1 | 5 | 0.3375 | 0.36 | 89.57 | -92.16 | 0.97 |

### *3.3.3 Amorphous vs. crystalline $WO_3$*

Figure 16 shows the CV of the same sample on FTO glass (I2) in three different stages: $TiO_2$ NTs (before $WO_3$ electrodeposition), amorphous $WO_3$ /$TiO_2$ NTs (after $WO_3$ electrodeposition and before annealing), and crystalline $WO_3$ /$TiO_2$ NTs (after $WO_3$ electrodeposition and after annealing). Bare $TiO_2$ NTs showed the lowest current density. crystalline $WO_3$ /$TiO_2$ NTs showed higher current density than amorphous $WO_3$ /$TiO_2$ NTs. However, Benoit et al. found that the charge density is slightly decreased due to the crystallinity of $WO_3$ nanoparticles [8]. The discrepancy could be due to the different synthetic approaches used that yield to different morphologies. The approach used in Bernoit's work was the decoration of $TiO_2$ nanotube layers with $WO_3$ nanoparticles by the controlled hydrolysis of a $WCl_6$ precursor. The final materials are open $TiO_2$ nanotubes covered with a hazy very thin $WO_3$ layer. Our approach creates completely different defined $WO_3$ nanostructures, including nanorods, nanowires and coral-like structures. In our case, the annealing step increases the ion uptake efficiency.

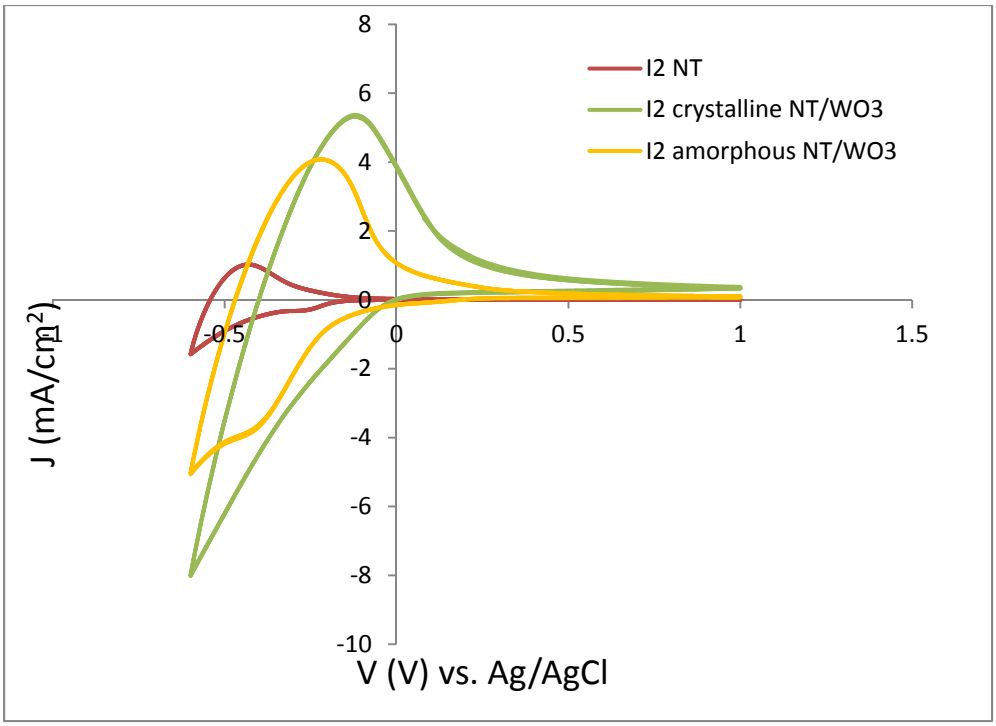


**Figure 16.** Sample I2 CV between 1 V and -0.6 V in 0.1 M $HClO_4$ electrolyte solution at a scan rate of 40 mV $s^{-1}$.

### *3.3.4 Cycling stability*

One important material property for any EC application is material stability over long periods of time. To the study the stability of these composite materials, CVs with 50 cycles were carried out. The charge capacities, peak positions, and peak ratios are summarized in Table 6. As shown in Figure 17 and Table 6, the charge capacity and redox reversibility of $WO_3$ materials quickly decreases in the first few cycles, and then stabilizes. The biggest changes can be seen during the first 5 cycles. The anodic and cathodic peaks become less defined and the ratio between the peaks changes from 0.37 to 0.24. When $WO_3$ is electrodeposited on FTO ($WO_3$/FTO), the film has poor stability. After several cycles using $WO_3$/FTO, blue, partially reduced $WO_3$ particles spontaneously detached from the FTO glass (Figure 18, left) and similar $WO_3$ particles can be seen at bottom of the electrochemical cell (Figure 18, right).

**Table 6.** The charge capacity and peak position after 50 cycles. Data calculated from CV in 0.1 M $HClO_4$ electrolyte solution at a scan rate of 40 mV $s^{-1}$.

| Sample | Cycles | $Q_{anodic}$ ($mC/cm^2$) | Anodic peak position (V) | $Qc_{cathodic}$ ($mC/cm^2$) | Cathodic peak position (V) | $Q_{anodic}/Q_{cathodic}$ |
|---|---|---|---|---|---|---|
| $WO_3$ | 1 | 3.63 | 0.019 | -9.822 | -0.511 | 0.37 |
| | 50 | 0.814 | 0.193 | -3.357 | -0.599 | 0.24 |
| $TiO_2$ NTs | 1 | 4.057 | -0.511 | -5.211 | -0.599 | 0.78 |
| | 50 | 0.251 | -0.194 | -17.21 | -0.599 | 0.01 |
| $TiO_2$ NTs / $WO_3$ (5h) | 5 | 68.49 | -0.176 | -74.01 | -0.599 | 0.93 |
| | 50 | 73.24 | -0.176 | -76.42 | -0.599 | 0.96 |

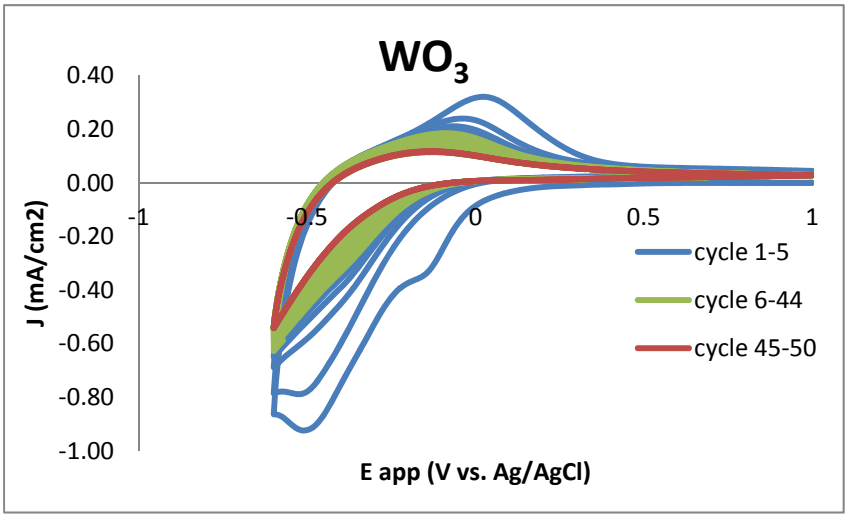


**Figure 17.** Fifty-cycle CV of $WO_3$/FTO in 0.1 M $HClO_4$ electrolyte solution at a scan rate of 40 mV $s^{-1}$.

**Figure 18.** $WO_3$ electrodeposited on FTO (left) and electrolyte solution after multiple CVs (right).

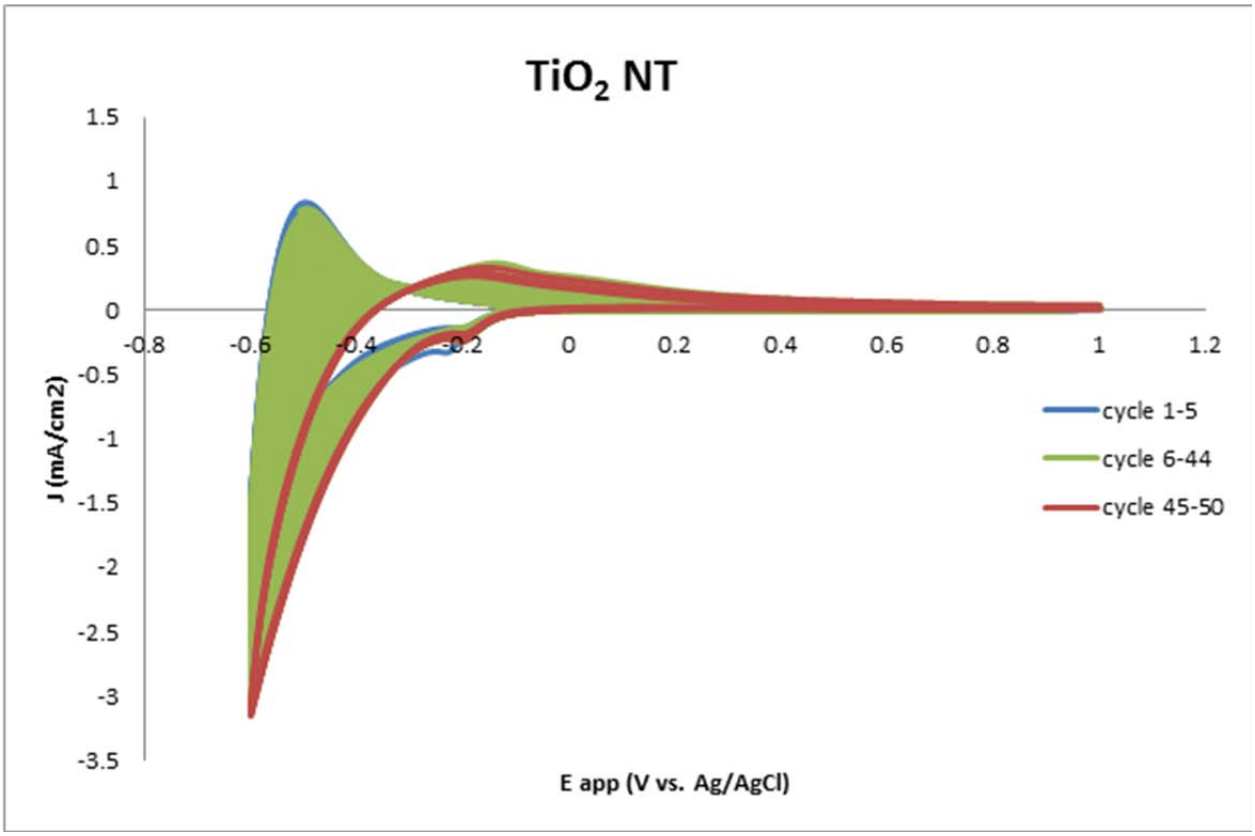


**Figure 19.** Fifty-cycle CV using $TiO_2$ NTs in 0.1 M $HClO_4$ electrolyte solution at a scan rate of 40 mV $s^{-1}$.

The $TiO_2$ NT films appeared visually identical after 50 cycles, with no evidence of detachment or degradation. However, as shown in Figure 19 and Table 6, anodic peak position shifted to a positive potential and the reversibility significantly decreased as a function of number of cycles. These results suggest a progressive irreversible intercalation in the $TiO_2$ lattice. On the contrary, the $WO_3$ film electrodeposited on $TiO_2$ NTs are very stable. After CVs using $WO_3/TiO_2$ NTs, the electrolyte solution and the bottom of the cell were always clear. Some of the $WO_3/TiO_2$ NTs have been used for multiple experiments and the performance has been very consistent. Figure 20 indicates that, after the first cycle, the following CVs showed very small differences, indicating high stability and durability. The ratio between the anodic and cathodic peaks moved from 0.93 to 0.96, indicating that the reversibility was even better after multiple cycles. XRD patterns (Figure 21) show that the crystal structure of the $WO_3/TiO_2$ NT materials was the same before and after the proton intercalation.

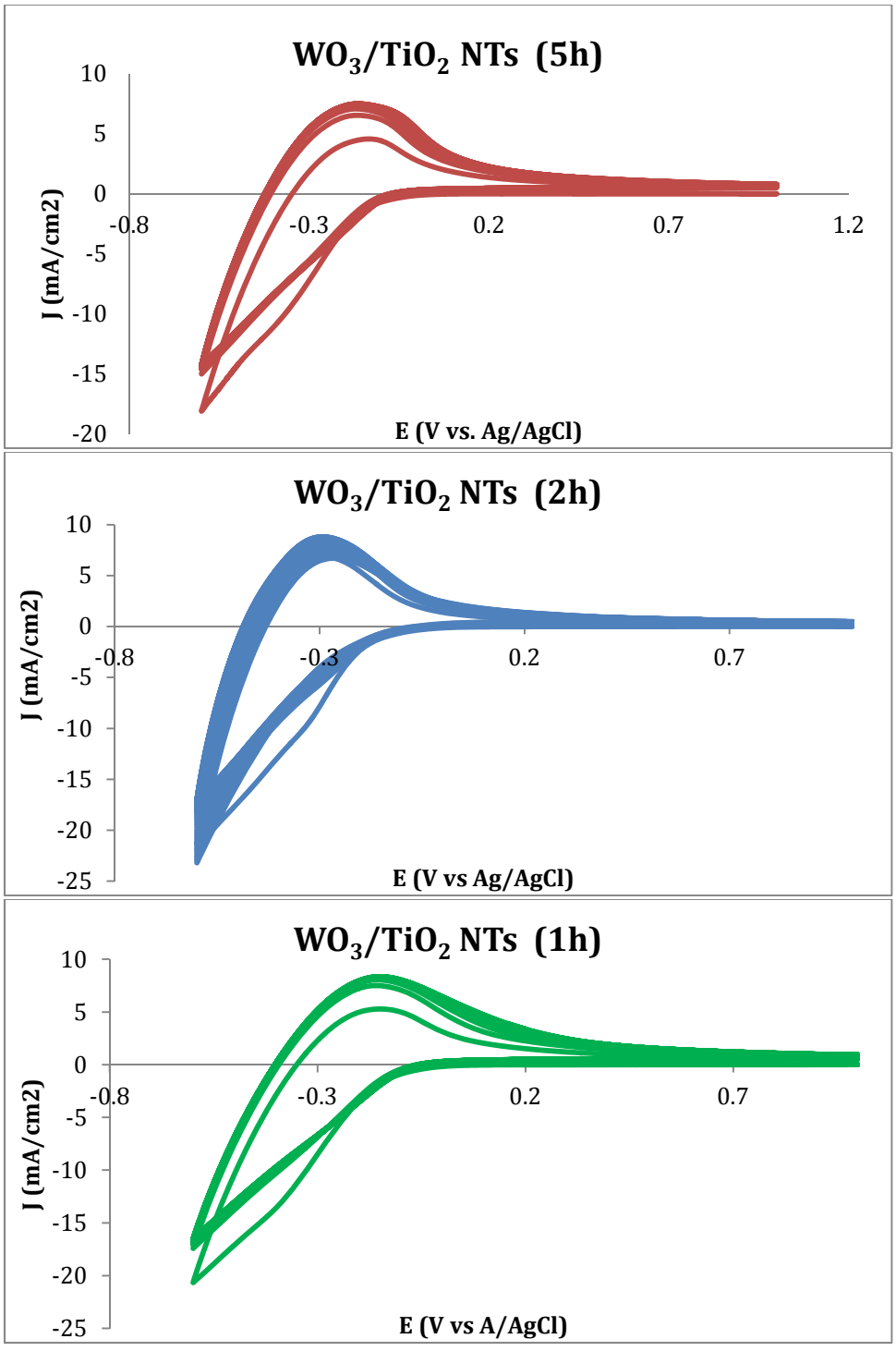


**Figure 20.** Fifty-cycle CVs using $WO_3/TiO_2$ NTs on FTO glass with different anodization times in 0.1 M $HClO_4$ electrolyte solution at a scan rate of 40 mV $s^{-1}$.

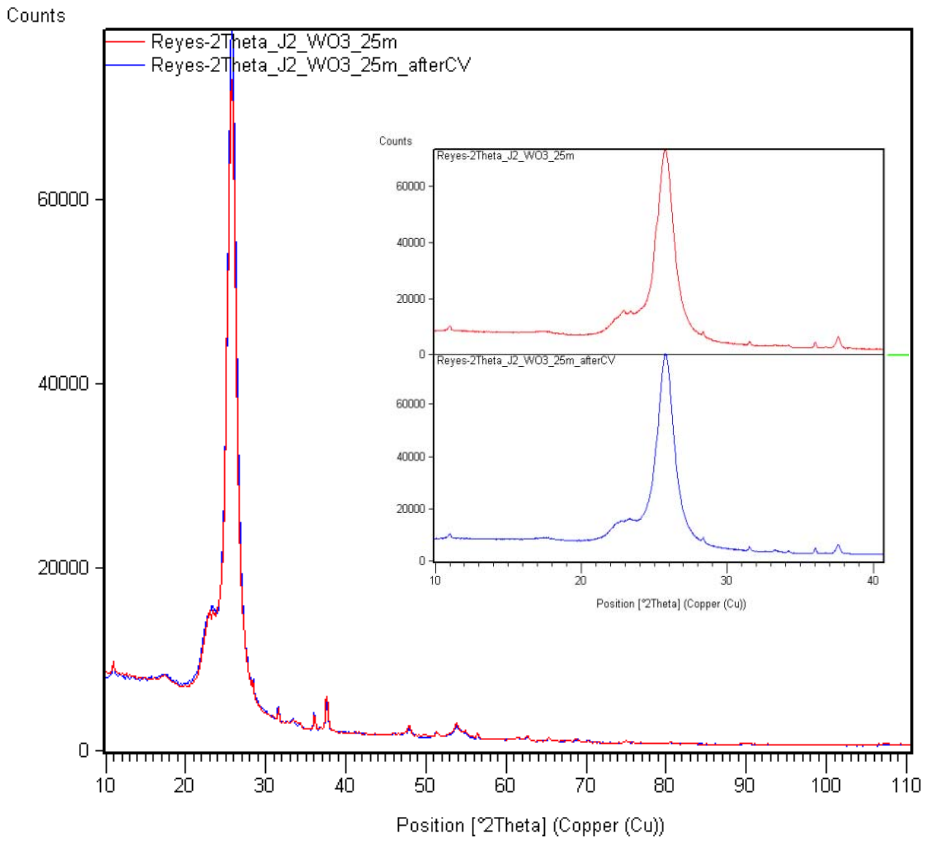


**Figure 21.** XRD of $WO_3$/ $TiO_2$ NTs on FTO glass before (red) and after (blue) CV.

### *3.3.5 Switching speed*

"Switching speed" is how fast the EC materials go from a colored to bleached state when voltage is applied. Double potential step chronoamperometry (DPSC) was used to compare the switching speeds of different $TiO_2$ NTs and $WO_3/TiO_2$ NT membranes on FTO glass. The films were cycled, alternating the potential from -1 V to 1 V for 5 s intervals. The cathodic current densities correspond to the film darkening as protons and charge-balancing electrons move into the film. The anodic current densities correspond to the film bleaching. As shown in Figure 22(a), the composite $WO_3/TiO_2$ NTs showed the largest charge density compared with pure $WO_3$ and $TiO_2$ NTs. In particular, $WO_3/TiO_2$ NTs 2 h (~15 µm nanotubes) showed the largest ion capacity while maintaining a fast switching speed (approximately 1 s to reach steady-state). For smart windows applications, switching speeds on the order of seconds are adequate. However, for other applications (such as displays), switching speeds on the order of milliseconds are needed. Figure 22 shows that $TiO_2$ NTs has a very fast response; however, a thick P25 nanoparticle layer has a significant slower switching speed. This observation suggests that the nanostructure could play an important role in determining the switching speed. In the case of $WO_3/TiO_2$ NTs, the P25 layer used as the adhesion layer could be increasing the switching time. In order to accelerate the switching time of $WO_3/TiO_2$ NTs, different adhesion layers (or thickness reduction of the P25 layer) should be investigated.

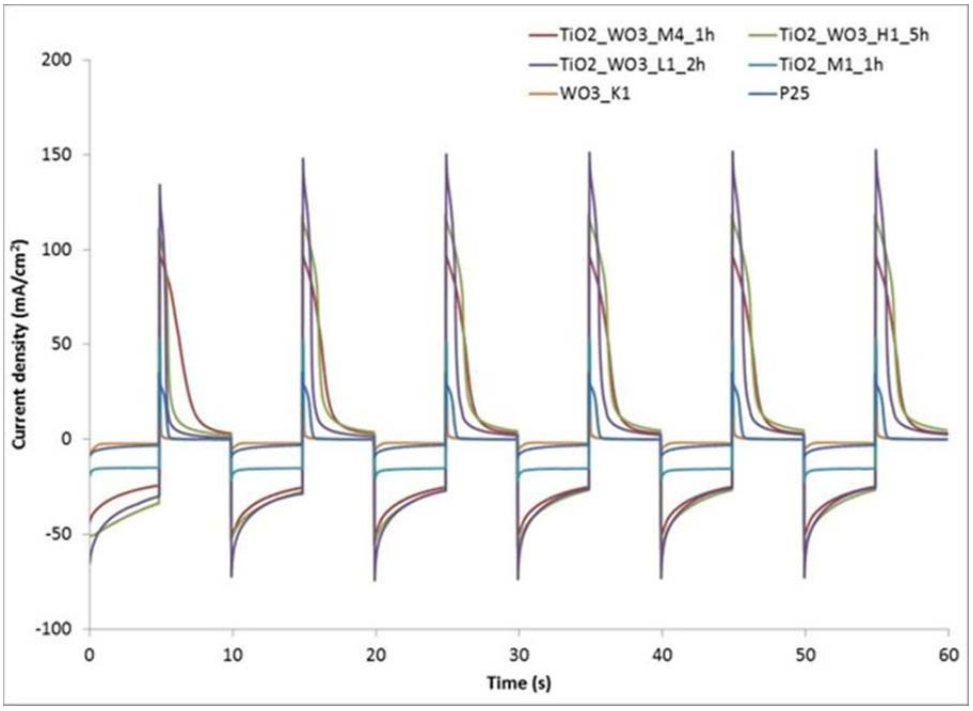


**(a)**

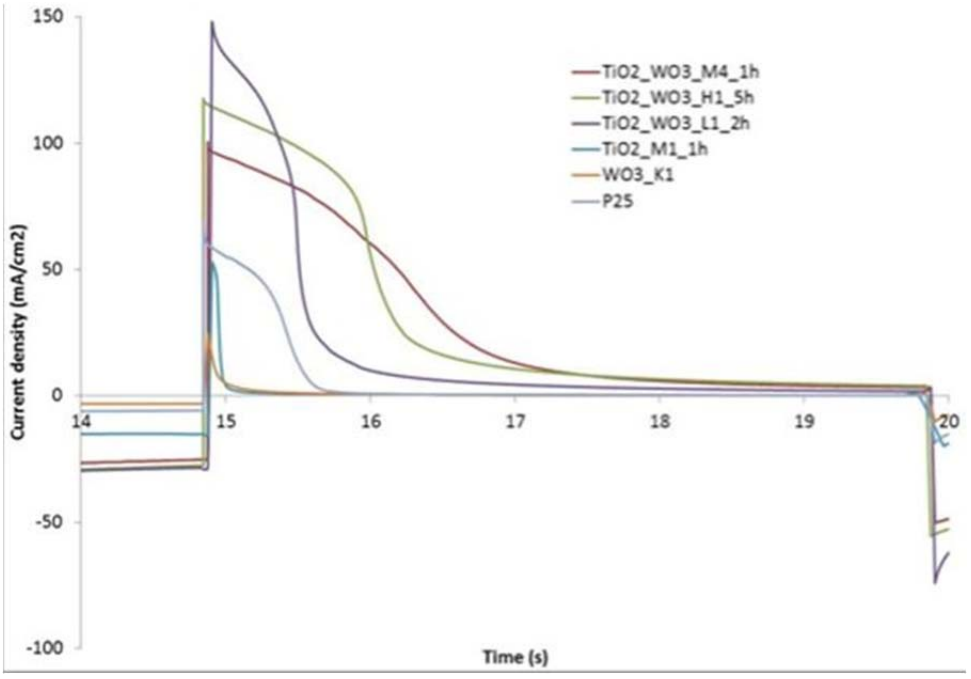


**(b)**

**Figure 22.** Alternating cycles from -1 V to 1 V for 5 s intervals in 0.1 M $HClO_4$ electrolyte solution at a scan rate of 40 mV $s^{-1}$.

### *3.3.6 Electrochromic contrast*

The change in redox state can be correlated quantitatively with changes in optical properties. Table 7 lists the samples used for the diffuse reflectance experiments**,** K1 is FTO glass with $WO_3$ electrodeposited on it, and the remainder of the membranes are composite materials of $TiO_2$ NTs attached with P25 paste onto FTO glass and $WO_3$ electrodeposited on the surface. For each of the samples in the following figures, a photograph was taken and the diffuse reflectance spectrum was collected before the electrochromic testing in order to demonstrate the initial state of the sample. Therefore, each sample was scanned anodically from 1 V to -0.6 V at 40 mV $s^{-1}$ in 0.1 M $HClO_4$ electrolyte solution. Another photograph was taken and the sample was placed inside the spectrometer as quickly as possible (around 5 min). Diffuse reflectance plots were shifted to match the initial diffuse reflectance of the material in the ultraviolet region to account any change due to sample loading or drying. Reflectance difference is the difference between the initial diffuse reflectance and the diffuse reflectance directly after the coloration cycle.

**Table 7.** Membranes used for diffuse reflectance analysis.

| Membrane | Material | Anodization time (h) | $WO_3$ electrodeposition (mA h $cm^{-2}$) |
|---|---|---|---|
| I3 | $TiO_2$ NTs | 5 h | ------ |
| I2 | $WO_3/TiO_2$ NTs | 5 h | 0.225 |
| H4 | $WO_3/TiO_2$ NTs | 2 h | 0.225 |
| J3 | $WO_3/TiO_2$ NTs | 1 h | 0.225 |
| K1 | $WO_3$ | N/A | 0.225 |

In the following figures, the diffuse reflectance spectra were plotted versus wavelength. The reflectance difference and photographs of the initial and final coloration states are included. Figure 23 shows that the electrochromic contrast of the reduced vs. oxidized $TiO_2$ NTs is almost negligible. However, Figure 24 shows that $WO_3$ film has a high electrochromic contrast. After the proton intercalation the film changes from transparent to blue. The diffuse spectra show a gradual increase in absorption from 450 nm to a maximum of approximately 750 nm.

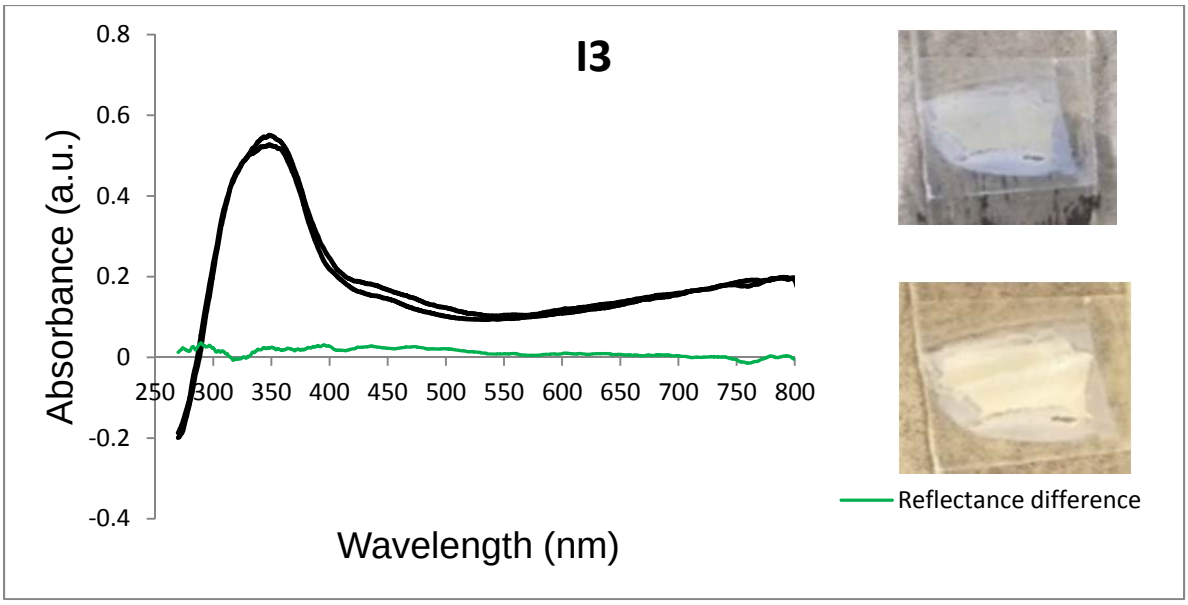


**Figure 23.** Spectral absorbance and photographs of a $TiO_2$ NT sample (I3) with 5 h anodization time before and after a coloration cycle.

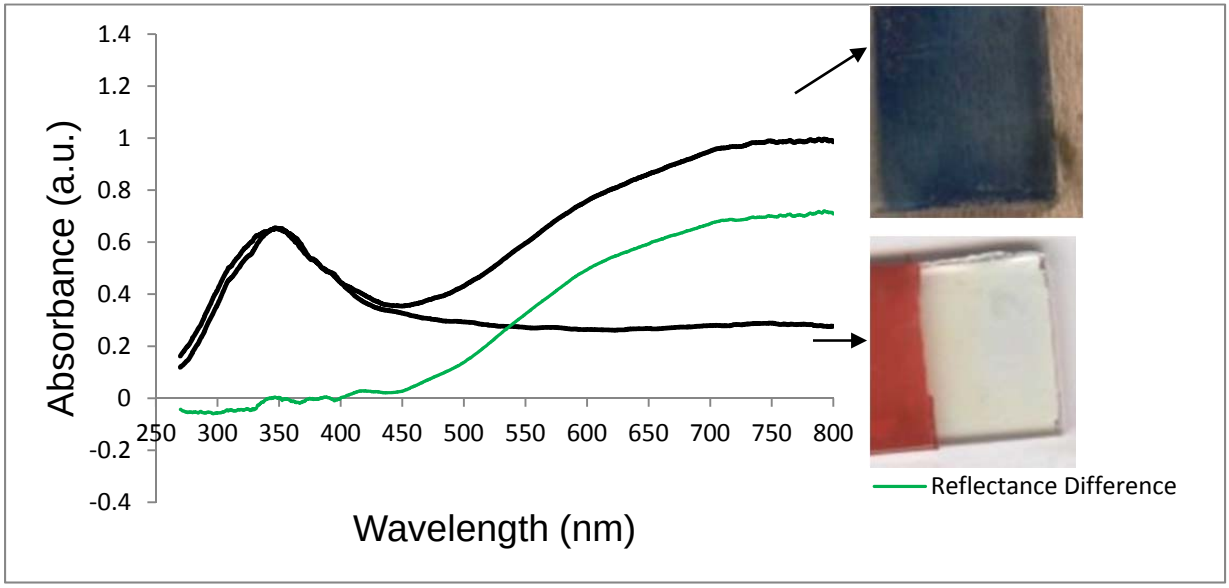


**Figure 24.** Spectral absorbance and photographs of $WO_3$ on FTO glass with a concentration of 0.225 mA h $cm^{-2}$ before and after a coloration cycle.

The following figures show the electrochromic contrast of composite $WO_3/TiO_2$ prepared with $TiO_2$ NTs with different anodization times. The post-coloration cycle photographs show that the material changed to a very dark color. Compared to $WO_3$ on FTO glass, the diffuse spectra show a flat absorption throughout the entire visible range (400–800 nm).

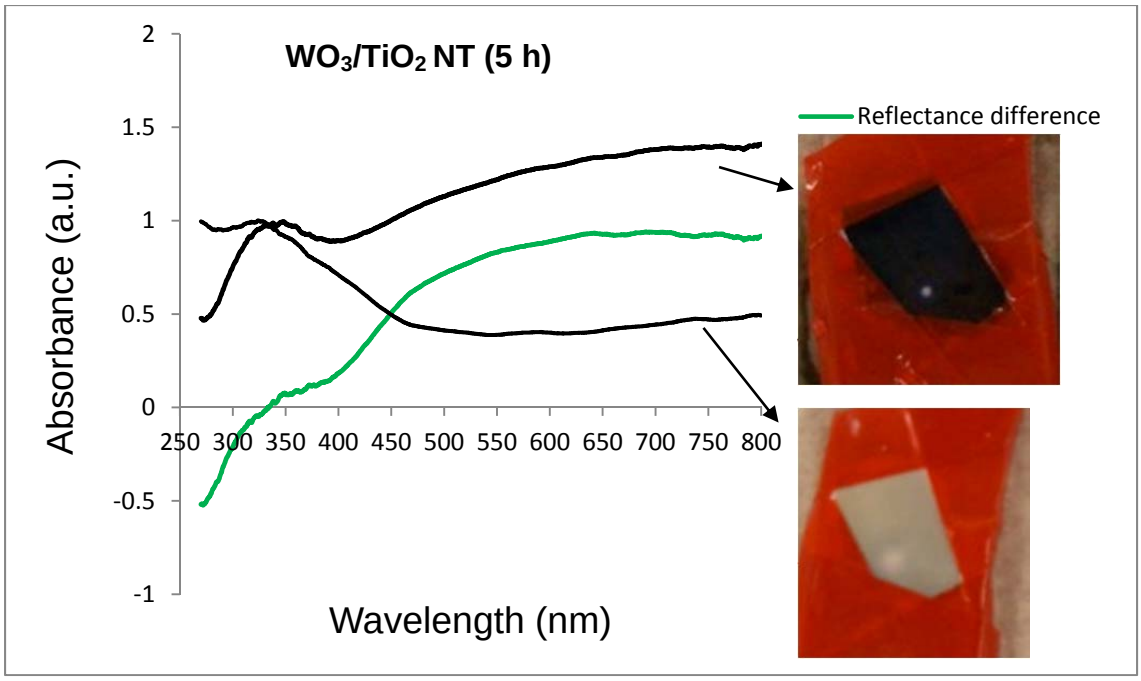


**Figure 25.** Spectral absorbance and photographs of a $WO_3/TiO_2$ NT membrane with 5 h anodization time and a $WO_3$ concentration of 0.225 mA h $cm^{-2}$ before and after a coloration cycle.

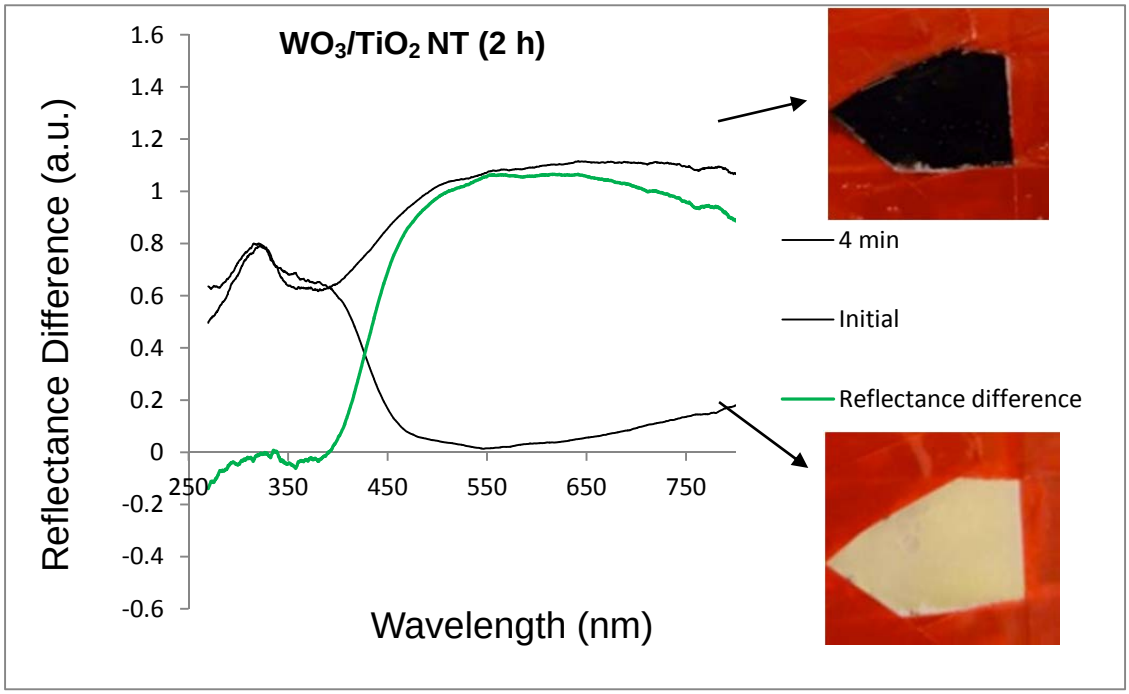


**Figure 26.** Spectral absorbance and photographs of a $WO_3/TiO_2$ NT membrane with 2 h anodization time and a $WO_3$ concentration of 0.225 mA h $cm^{-2}$ before and after a coloration cycle.

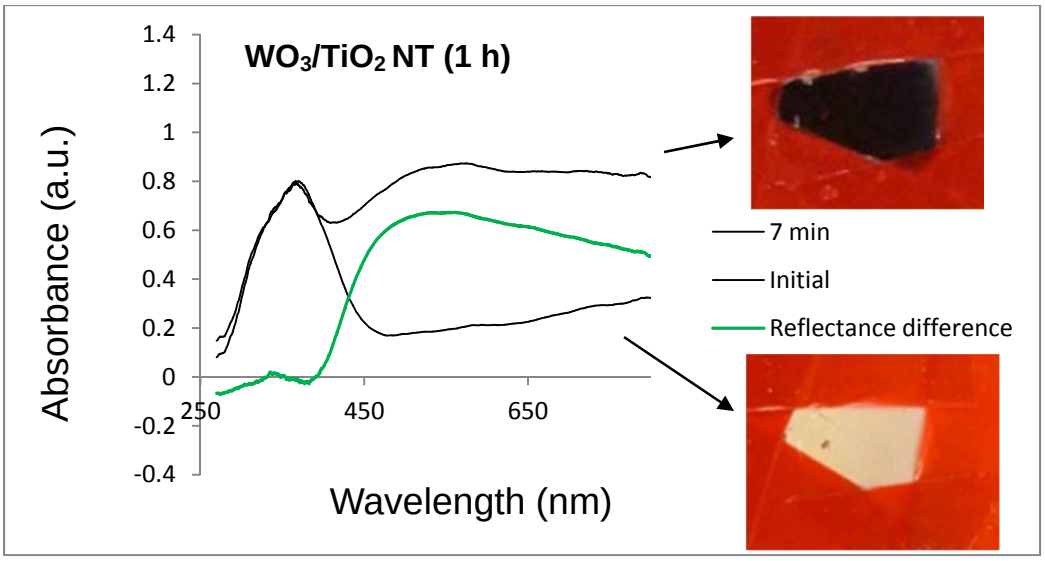


**Figure 27.** Spectral absorbance and photographs of a $WO_3/TiO_2$ NT membrane with 1 h anodization time and a $WO_3$ concentration of 0.225 mA h $cm^{-2}$ before and after a coloration cycle.

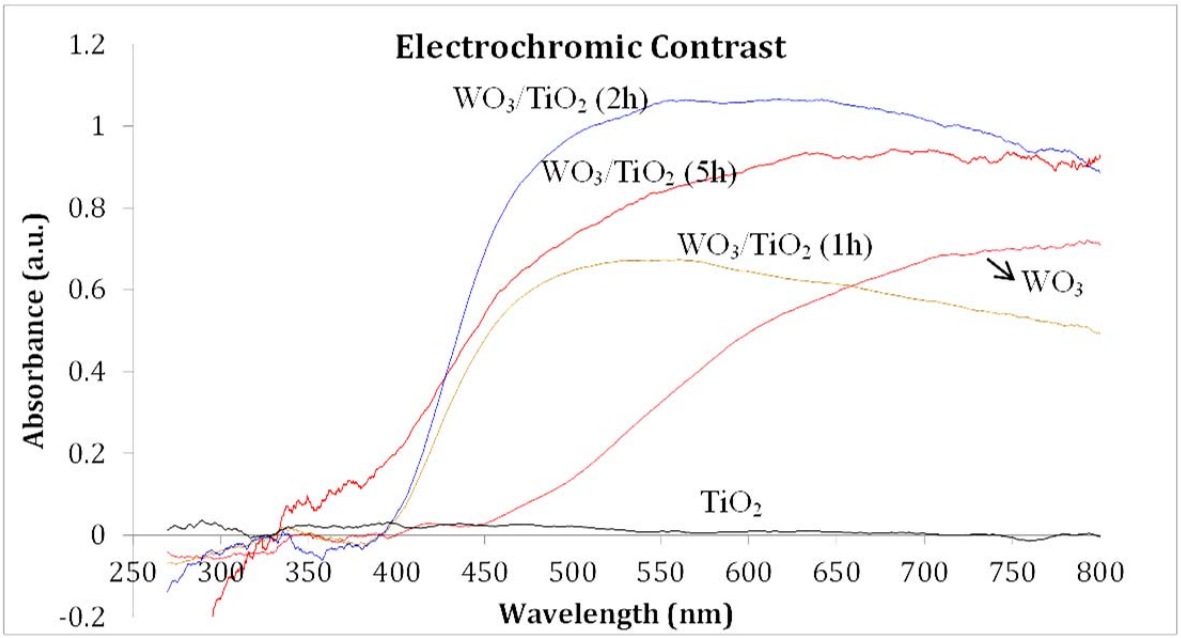


**Figure 28.** Overlay of change in absorbance for samples in Figures 23-27.

Figure 28 compares the electrochromic contrast of all the samples. The EC contrast for bare $TiO_2$ is negligible. Bare $WO_3$ has a significant EC contrast only at longer wavelengths. However, the combination of these two materials has a big impact in EC in terms of the wavelength range.. $WO_3/TiO_2$ materials show a constant maximum EC contrast from 450 nm to 800 nm. Figure 28

indicates that the largest EC contrast is the $WO_3/TiO_2$ NTs (2 h) material. In the previous section, we showed that the length of NTs has small effect on the current density; however, figure 28 indicates that it has a bigger effect on the change in reflectance.

### *3.3.7 Memory: shift time from colored to bleached state with no applied voltage*

For some EC applications, such as smart windows, materials with a long memory time at open circuit are desirable because they can retain color for long periods without the need to re-apply voltage. In this section, we used the in situ diffuse reflectance data collected at different time intervals (approximately every 5 min). Figure 29 shows how the absorption changes as a function of time from 5 minutes after the coloration cycle to back to the initial state (350 min for $WO_3/TiO_2$ prepared with $TiO_2$ NTs anodized during 1 h). This type of data was collected for all the samples shown in Table 8.

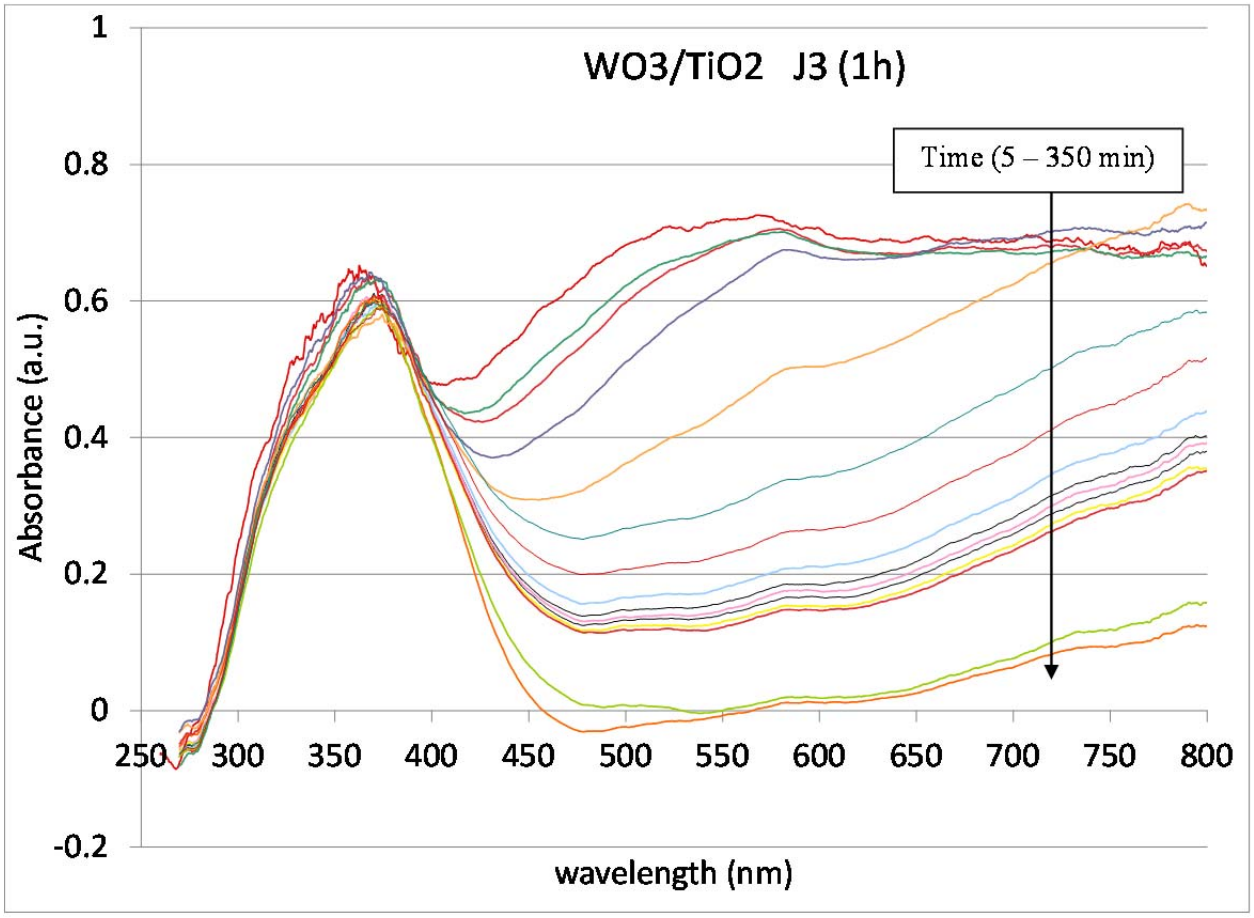


**Figure 29.** Diffuse reflectance spectra for $WO_3/TiO_2$ collected in situ from 5 to 350 min with a 23-minute interval between spectra.

Diffuse reflectance data was plotted at constant wavelength of 600 nm versus time. Figure 30 indicates that $WO_3$ followed by $WO_3/TiO_2$ NTs (1 h), $WO_3/TiO_2$ NTs (2 h) and finally $WO_3/TiO_2$ NTs (5 h) changes color the fastest directly after anodic bias. This result indicates that the NTs increase the materials' abilities to retain charge relative to the nanoparticulate $WO_3$. Moreover, the length of NTs is directly proportional to the memory time.

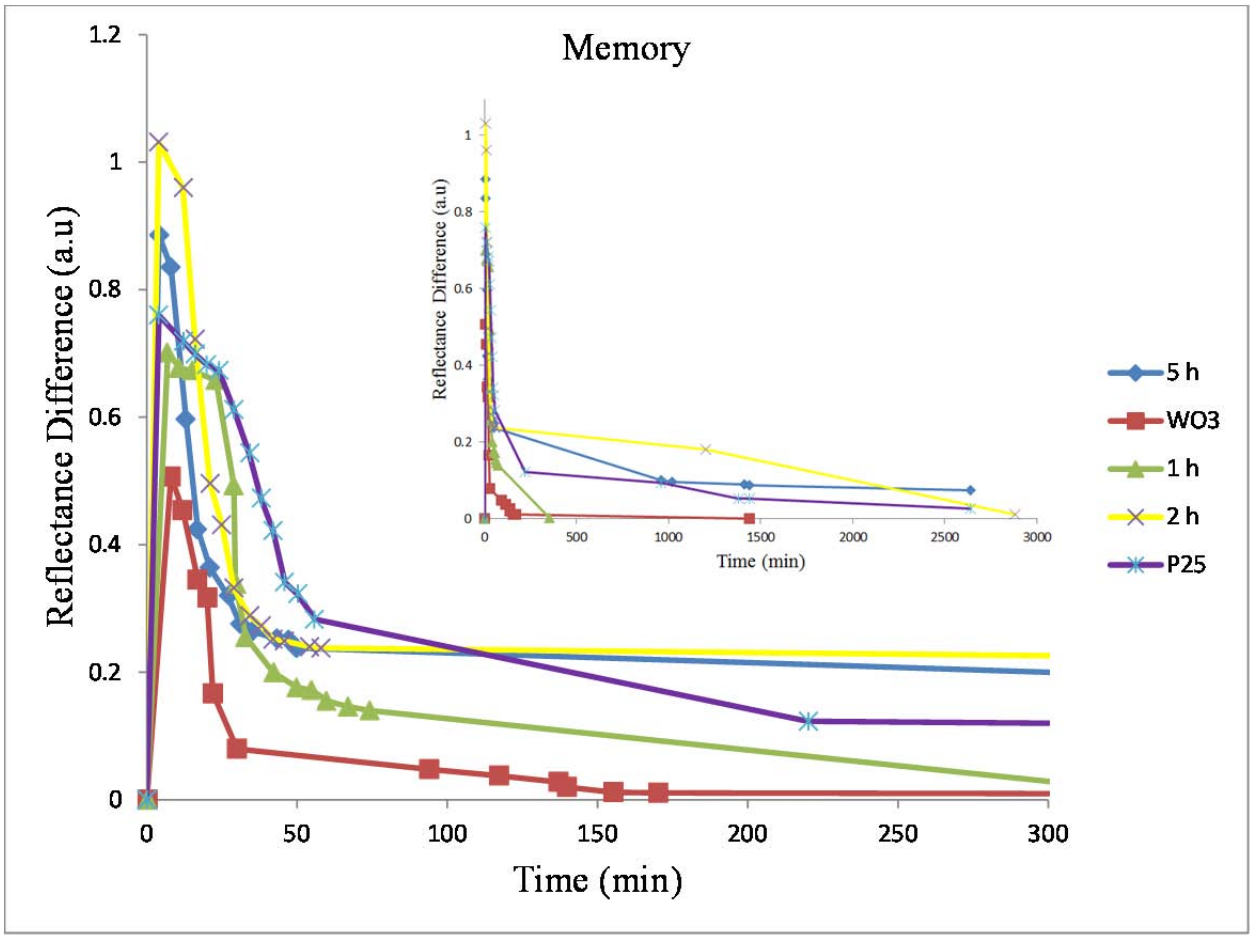


**Figure 30.** Reflectance difference vs. time at 600 nm with data points taken after a CV experiment scanning from 1 V to -0.6 V at 40 mV $s^{-1}$ in 0.1 M $HClO_4$ electrolyte solution. The inset graphically shows the data in Table 8.

**Table 8.** Final reflectance difference calculated after an extended period of time.

| Sample | Reflectance Difference (a.u.) | Time (h) |
|---|---|---|
| K1 ($WO_3$) | 0.005 | 3 |
| J3 (1 h) | 0.004 | 6 |
| H4 (2 h) | 0.012 | 44 |
| I2 (5 h) | 0.074 | 44 |

Table 8 summarizes the final reflectance difference of the materials after anodic polarization. At 44 h, neither the $WO_3/TiO_2$ NTs (2 h), nor the $WO_3/TiO_2$ NTs (5 h), have completely reversed back to their initial states. After 6 h the $WO_3/TiO_2$ NT (1 h) material and the $WO_3$ on FTO glass have very small values of reflectance difference. This result is in accord with observations that the materials with the 1 h NTs revert back to their initial state faster than the materials with longer NTs. For these spectroscopy measurements, the electrodes are in open circuit conditions outside of the electrolyte and exposed to air. Under these uncontrollable conditions, several factors could affect the memory time including reactions with $O_2$ and drying conditions. In order to have more reliable results, controlled atmosphere (Ar gas) or in situ measurements are needed.

### *3.3.8 Relative diffusion of intercalated ion*

In cyclic voltammetry, the Randles-Sevcik equation describes the peak current density ($i_p$) dependence on the concentration and diffusional properties of the electroactive species:

$$i_p = 0.4463\ nFAC(nFvD/RT)^{1/2}$$

or, if the solution is at room temperature:

$$i_p = (269{,}000)n^{3/2}AD^{1/2}Cv^{1/2}$$

where $i_p$ is current maximum in amps, $n$ is number of electrons transferred in the redox event, $A$ is electrode area in $cm^2$, $F$ is the Faraday constant in C $mol^{-1}$, $D$ is diffusion coefficient in $cm^2/s$, $C$ is concentration in $mol/cm^3$, and $v$ is scan rate in V/s. This equation assumes that the current is limited by diffusion from a very thick or semi-infinite layer to a planar electrode surface.

Also, the peak current density is dependent on scan rate, but the charge is independent. Based on the Randeles-Sevcik equation, $i_p$ is expected to increase at faster voltage scan rates. Current is defined as charge (or electrons passed) per unit time. Therefore, at faster voltage scan rates the charge passed per unit time is greater, hence, an increase in $i_p$, while the total amount of charge is the same. Using the relationships defined by this equation, the diffusion coefficient of the electroactive species can be determined. Figures 31 to 35 show the peak anodic current's dependence on the scan rate. A linear dependence of oxidative peak current on the square root of the scan rate indicates a diffusion limited redox reaction [18]. Linear plots of $i_p$ vs. $v^{1/2}$ provide evidence for a chemically reversible redox process vs. the cases where redox causes major structural change in the analyte. The following figures show that with this type of material, the redox reaction is mass transfer limited as opposed to kinetically limited.

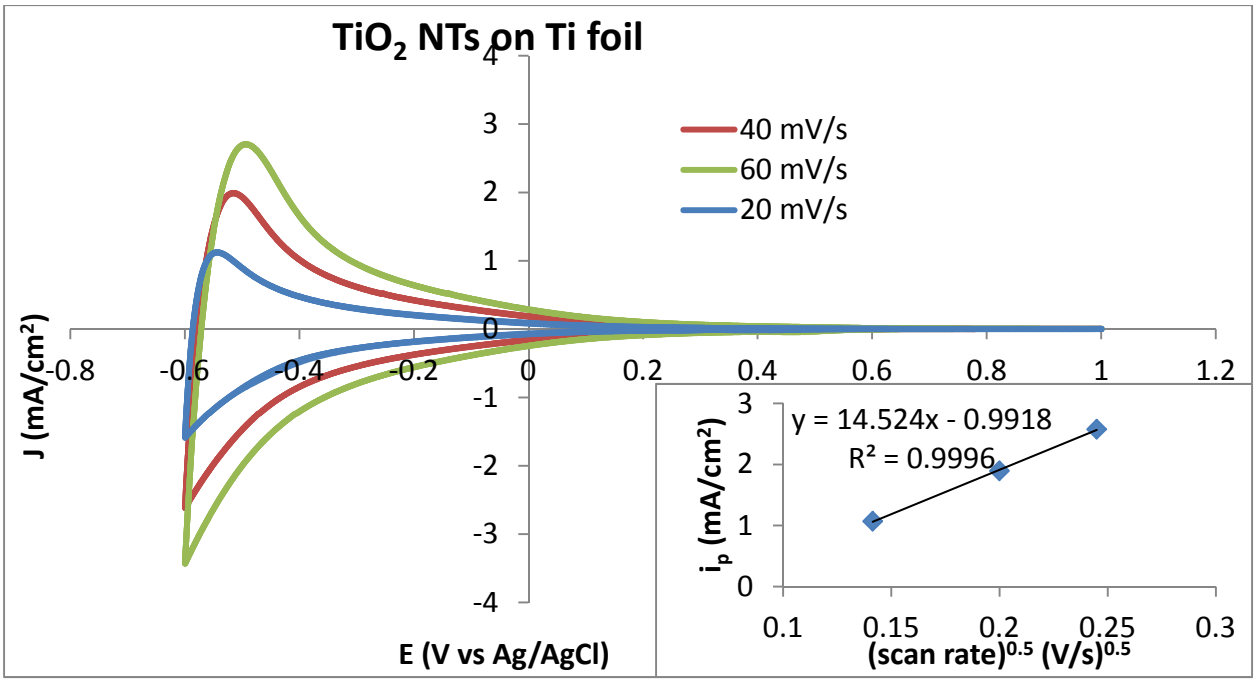


**Figure 31.** Comparison of CVs between 1 V and -0.6 V in 0.1 M $HClO_4$ electrolyte solution at different scan rates for $TiO_2$ NTs on Ti foil. The inset shows the dependence of peak anodic current ($i_p$) on the square root of the scan rate.

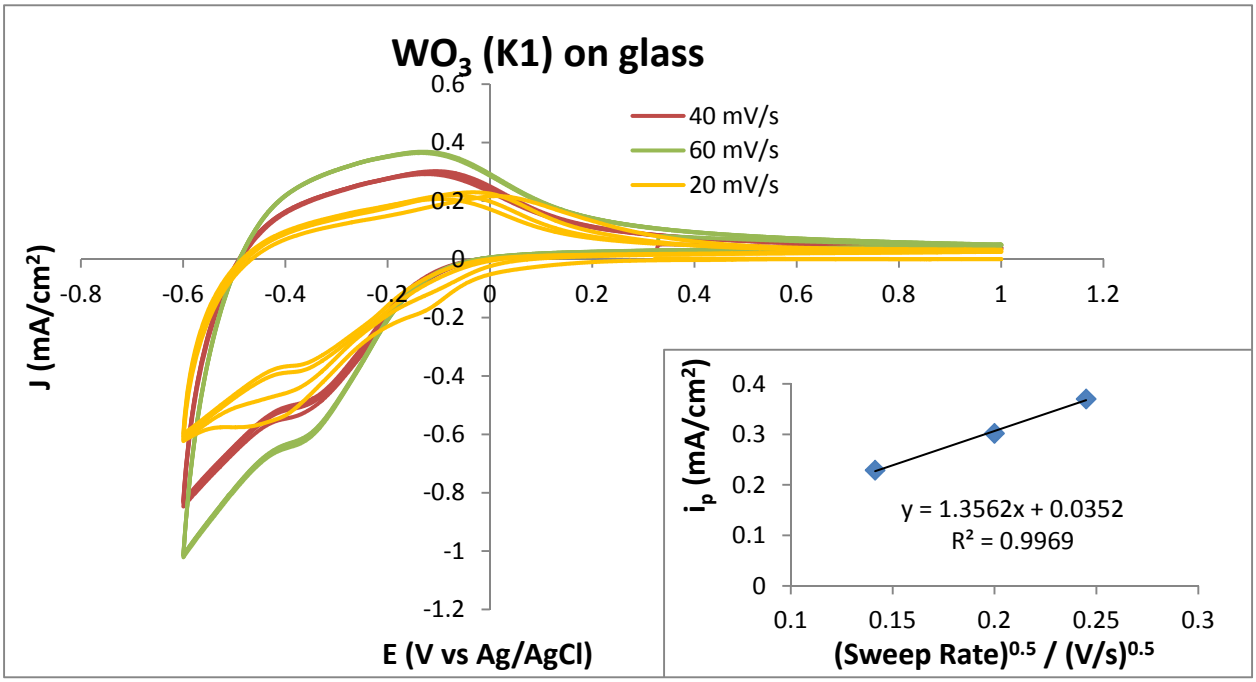


**Figure 32.** Comparison of CVs between 1 V and -0.6 V in 0.1 M $HClO_4$ electrolyte solution at different scan rates for $WO_3$ crystalline on FTO glass. The inset shows the dependence of peak anodic current ($i_p$) on the square root of the scan rate.

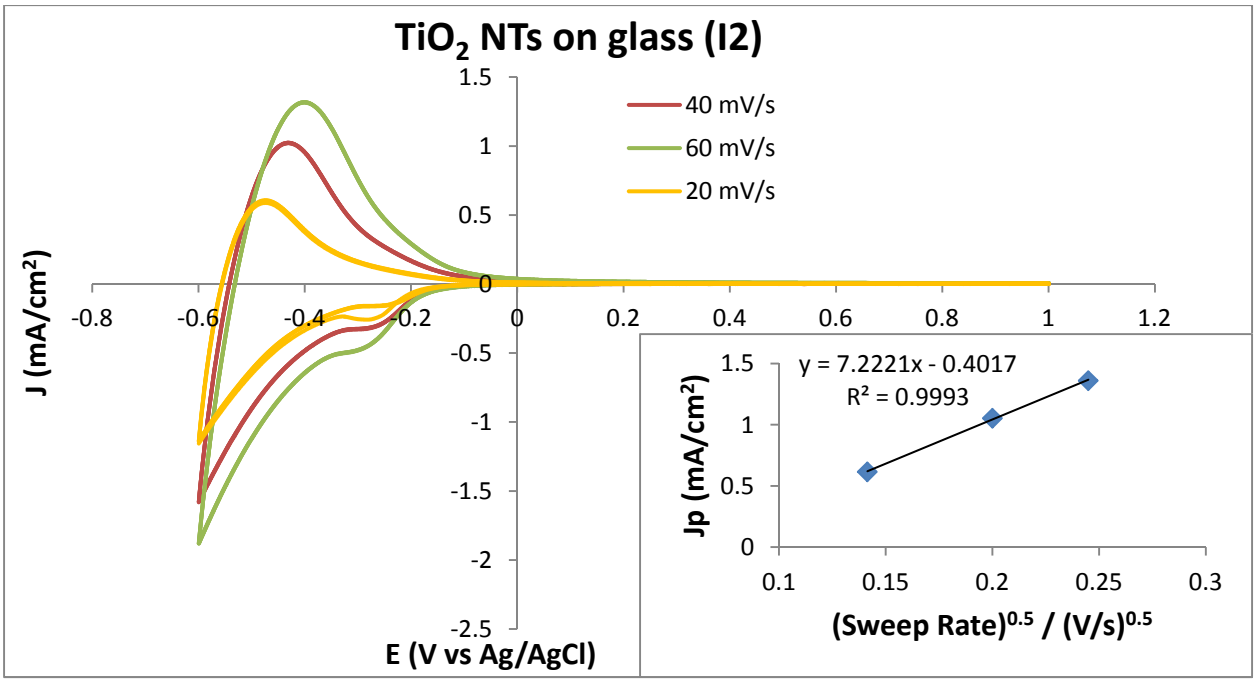


**Figure 33.** Comparison of CVs between 1 V and -0.6 V in 0.1 M $HClO_4$ electrolyte solution at different scan rates for $TiO_2$ NTs on FTO glass. The inset shows the dependence of peak anodic current ($i_p$) on the square root of the scan rate.

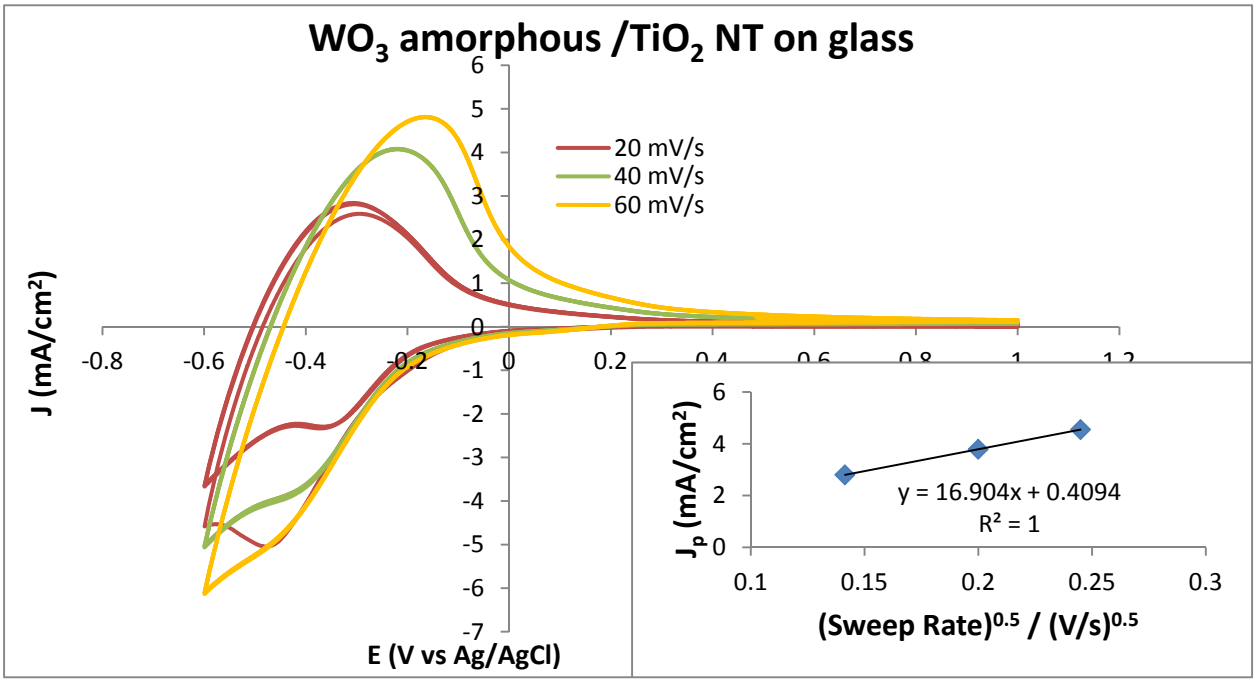


**Figure 34.** Comparison of CVs between 1 V and -0.6 V in 0.1 M $HClO_4$ electrolyte solution at different scan rates for $WO_3$ amorphous/$TiO_2$ NTs on FTO glass. The inset shows the dependence of peak anodic current ($i_p$) on the square root of the scan rate.

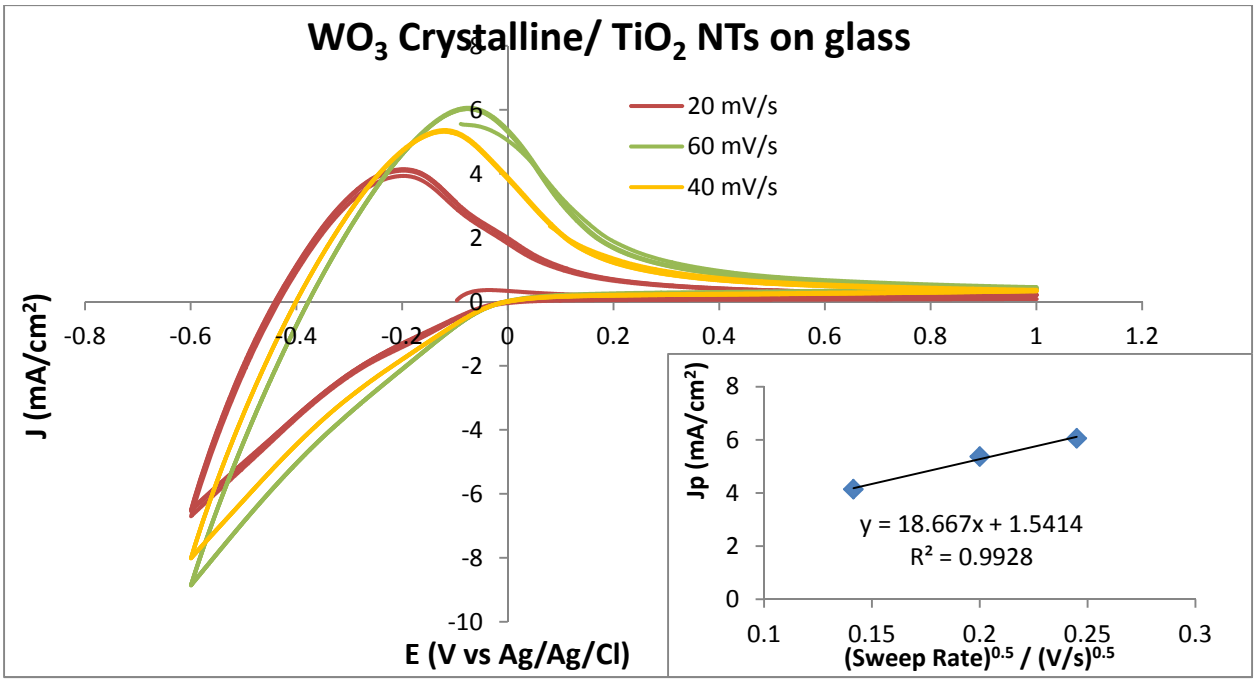


**Figure 35.** Comparison of CVs between 1 V and -0.6 V in 0.1 M $HClO_4$ electrolyte solution at different scan rates for $WO_3$ crytalline / $TiO_2$ NT on FTO glass. The inset shows the dependence of peak anodic current ($i_p$) on the square root of the scan rate.

The Randles-Sevcik equation assumes that the diffusion of the oxidative process and the diffusion of the reduction process are equal. According to Ozer [19], the redox reaction is not fully reversible as some intercalated ions bind irreversibly to $TiO_2$ upon cathodic bias. However, for some of our composite materials, we found charge ratios as high as 0.97. Therefore, we assume that even though our materials are not 100% reversible, the reversibility is high enough to use the Randles-Sevcik equation to calculate the diffusion coefficient. Table 9 summarizes the diffusion coefficient calculated using the Randles-Sevcik equation at each scan rate. Also, the diffusion coefficient was calculated using the slope of $i_p$ vs. scan rate$^{1/2}$ plot.

For the single materials ($TiO_2$ and $WO_3$), the diffusion coefficient decreases with decreasing scan rate, as reported previously for $WO_3$ materials [20]. On the other hand, for the composite materials, the diffusion coefficient increases with decreasing scan rate. The average of diffusion coefficients calculated at each scan rate and the value calculated using the slope of $i_p$ vs. scan rate$^{1/2}$ plot are slightly different but follow the same trend. $WO_3$ nanoparticles have the smallest diffusion coefficient followed by $TiO_2$ NT. The composites materials have the largest diffusion coefficients.

**Table 9.** Calculation of diffusion coefficient using Randles-Sevcik equation.

| Sample | Rate (mV/s) | Ip (A/cm$^2$) | D (cm$^2$/s) | D*(cm$^2$/s) |
|---|---|---|---|---|
| $WO_3$ | 60 | 0.00055 | 3.21E-09 | |
| | 40 | 0.00040 | 2.60E-09 | |
| | 20 | 0.00030 | 2.84E-09 | |
| | | | **(Average) 2.88E-09** | **6.09E-09** |
| $TiO_2$ NT (I2) | 60 | 0.00136 | 3.93E-08 | |
| | 40 | 0.00105 | 3.53E-08 | |
| | 20 | 0.00061 | 2.40E-08 | |
| | | | **(Average) 3.29E-08** | **3.88E-08** |
| $WO_3$(amorphous)/ $TiO_2$ NT (I2) | 60 | 0.00455 | 6.90E-07 | |
| | 40 | 0.00379 | 7.15E-07 | |
| | 20 | 0.00280 | 7.81E-07 | |
| | | | **(Average) 7.29E-07** | **4.94E-07** |
| $WO_3$(crystalline)/ $TiO_2$ NT (I2) | 60 | 0.00606 | 2.85E-06 | |
| | 40 | 0.00105 | 3.35E-06 | |
| | 20 | 0.00061 | 3.99E-06 | |
| | | | **(Average) 3.40E-06** | **9.42E-07** |

D* was calculated using the slope of $i_p$ vs. scan rate$^{1/2}$ plot.

# 4. Future work

## 4.1 Reuse of Ti foil

The Ti substrate can be reused for manufacture of several NT membranes sequentially after the membrane is separated, which makes it economical and environmentally favorable. As proof of concept, several scanning electron microscope (SEM) micrographs of the membranes, after sequential fabrication with the same Ti substrate, show little change to the morphology of the membranes [16].

## 4.2 Optimization of optical properties

To obtain more transparent membranes, the NT length has to be reduced to a few microns. As we showed in this work, when the NT length is reduced to ~6µm, the EC contrast is reduced. One proposed method to obtain transparent but high-EC contrast materials is to increase the $WO_3$ concentration. Although increasing the concentration of $WO_3$ did not show a significant improvement in the ion capacity storage, it did produce an enhancement in the electrochromic contrasts, as shown in Figure 36.

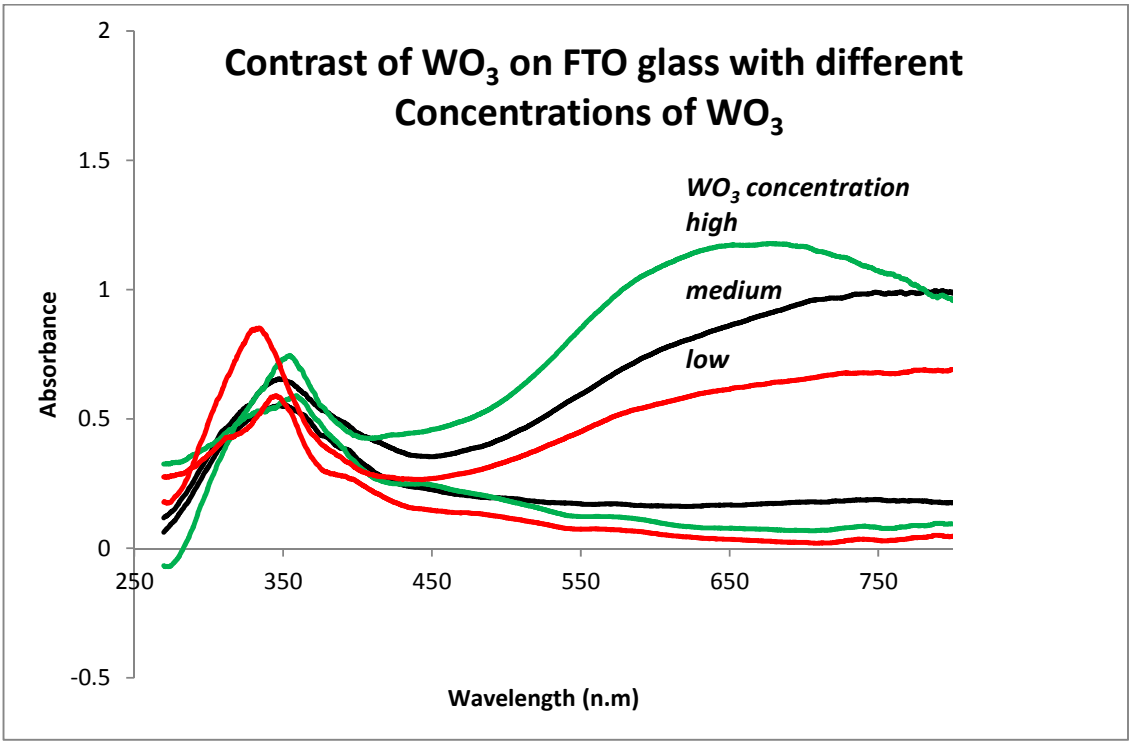


**Figure 36.** Electrochromic contrast of $WO_3$ with different concentrations on FTO glass.

# 5. Conclusions

In this work, we showed that $TiO_2$ nanotubes can be used for the development of composite $TiO_2/WO_3$ materials with unique organized nanostructures. The $TiO_2$ NTs act as a skeleton for the $WO_3$ electrodeposition. The $TiO_2$ NTs can be detached and successfully transferred to glass. The composite $WO_3/TiO_2$ nanostructures showed higher ion storage capacity and enhanced EC contrast compared with the pure $WO_3$ and $TiO_2$. Also, the composite materials showed excellent cycling stability. The EC redox reaction seen in this material is diffusion-limited. The composite materials showed the largest diffusion coefficient. The use of $TiO_2$ NTs as substrate may also have a significant impact on the electrodeposition of other materials.

# 6. References


1. Deb, S.K., *Photovoltaic-Integrated Electrochromic Device for Smart-Window Applications*, in *World Renewable Energy Congress VI*2000, National Renewable Energy Laboratory: Brighton, U.K.
2. Roy, P., S. Berger, and P. Schmuki, *$TiO_2$ Nanotubes: Synthesis and Applications.* Angewandte Chemie International Edition, 2011. **50**(13): p. 2904-2939.
3. Granqvist, C.G., *Handbook of Inorganic Electrochromic Materials*2002, Amsterdam: Elsevier.
4. M.S Monk, R.J.M., D.R. Rosseinsky, *Electrochromism: Fundamentals and Applications* 1995, Weinheim: VCH.
5. Yu, Z., et al., *Electrochromic $WO_3$ films prepared by a new electrodeposition method.* Solar Energy Materials and Solar Cells, 2000. **64**(1): p. 55-63.
6. Norma R. de Tacconi, C.R.C., Krishnan Rajeshwar, *Electrochromic behavior of $WO_3$, $TiO_2$, and composite $WO_3$-$TiO_2$ films prepared by pulsed electrodeposition.* Electrochemical Society Proceedings 2003. **17**: p. 28-39.
7. Nah, Y.-C., et al., *Enhanced electrochromic properties of self-organized nanoporous $WO_3$.* Electrochemistry Communications, 2008. **10**(11): p. 1777-1780.
8. Benoit, A., et al., *Decoration of $TiO_2$ nanotube layers with $WO_3$ nanocrystals for high-electrochromic activity.* Electrochemistry Communications, 2009. **11**(4): p. 728-732.
9. Lai, C.W., S. Sreekantan, and P. San E, *Effect of radio frequency sputtering power on W–$TiO_2$ nanotubes to improve photoelectrochemical performance.* Journal of Materials Research, 2012. **27**(13): p. 1695-1704.
10. Nah, Y.-C., et al., *$TiO_2$−$WO_3$ Composite Nanotubes by Alloy Anodization: Growth and Enhanced Electrochromic Properties.* Journal of the American Chemical Society, 2008. **130**(48): p. 16154-16155.
11. Ito, S., et al., *Fabrication of screen-printing pastes from $TiO_2$ powders for dye-sensitised solar cells.* Progress in Photovoltaics: Research and Applications, 2007. **15**(7): p. 603-612.
12. Li, L.-L., et al., *Detachment and transfer of ordered $TiO_2$ nanotube arrays for front-illuminated dye-sensitized solar cells.* Energy & Environmental Science, 2011. **4**(9): p. 3420-3425.
13. Albu, S.P., A. Ghicov, and P. Schmuki, *Lift Off Strategies for Self-Organized $TiO_2$ Nanotube Layers.* ECS Transactions, 2009. **16**(52): p. 195-202.
14. Albu, S.P., et al., *Self-Organized, Free-Standing $TiO_2$ Nanotube Membrane for Flow-through Photocatalytic Applications.* Nano Letters, 2007. **7**(5): p. 1286-1289.
15. Liu, G., et al., *A voltage-dependent investigation on detachment process for free-standing crystalline $TiO_2$ nanotube membranes.* Journal of Materials Science, 2011. **46**(24): p. 7931-7935.

16. Wang, D. and L. Liu, *Continuous Fabrication of Free-Standing $TiO_2$ Nanotube Array Membranes with Controllable Morphology for Depositing Interdigitated Heterojunctions.* Chemistry of Materials, 2010. **22**(24): p. 6656-6664.

17. Zanello, P., *Inorganic Electrochemistry* 2003, Cambridge UK: The Royal Society of Chemistry. 607.

18. Lindström, H., et al., *Li+ Ion Insertion in $TiO_2$ (Anatase). 2. Voltammetry on Nanoporous Films.* The Journal of Physical Chemistry B, 1997. **101**(39): p. 7717-7722.

19. Özer, N., *Reproducibility of the coloration processes in $TiO_2$ films.* Thin Solid Films, 1992. **214**(1): p. 17-24.

20. Leftheriotis, G., S. Papaefthimiou, and P. Yianoulis, *Dependence of the estimated diffusion coefficient of $LixWO_3$ films on the scan rate of cyclic voltammetry experiments.* Solid State Ionics 2007. **178**: p. 259-263.

# Distribution

| | | | |
|---|---|---|---|
| 4 | Lawrence Livermore National Laboratory<br>Attn: N. Dunipace<br>P.O. Box 808, MS L-795<br>Livermore, CA 94551-0808 | | |
| 1 | MS0899 | Technical Library | 9536 (electronic copy) |
| 1 | MS9291 | David B. Robinson | 8651 |
| 1 | MS9403 | Karla Reyes | 8223 |


Sandia National Laboratories